not differ among various spleen cells from CD150Tg, CD150Tg/*Ifnar*$^{-/-}$, CD150Tg/*Irf3*$^{-/-}$/*Irf7*$^{-/-}$, CD150Tg/*Ticam1*$^{-/-}$ or CD150Tg/*Mavs*$^{-/-}$ mice (Supplemental Fig. 1). Each knockout mouse strain was i.p. injected with 1×10^6 PFU of MV-luciferase. In accord with previous data (16, 22), luciferase activity in various tissues derived from MV-infected CD150Tg mice was very low 2 d after inoculation (Fig. 1A). In contrast, luciferase activity was predominantly increased in spleen and lymph nodes (LNs) derived from MV-infected CD150Tg/*Ifnar*$^{-/-}$ mice, compared with other tissues (Fig. 1A). *MV-P* mRNA expression was also increased in MV-infected CD150Tg/*Ifnar*$^{-/-}$ spleen and LNs, similarly to luciferase activity (Fig. 1B). These results indicate that spleen and LNs are the major target tissues of i.p.-injected MV in CD150Tg/*Ifnar*$^{-/-}$ mice, as shown in a previous report (24). Luciferase activity was increased in the lung of CD150Tg/*Ifnar*$^{-/-}$, but not CD150Tg/*Mavs*$^{-/-}$, mice after intratracheal injection of MV

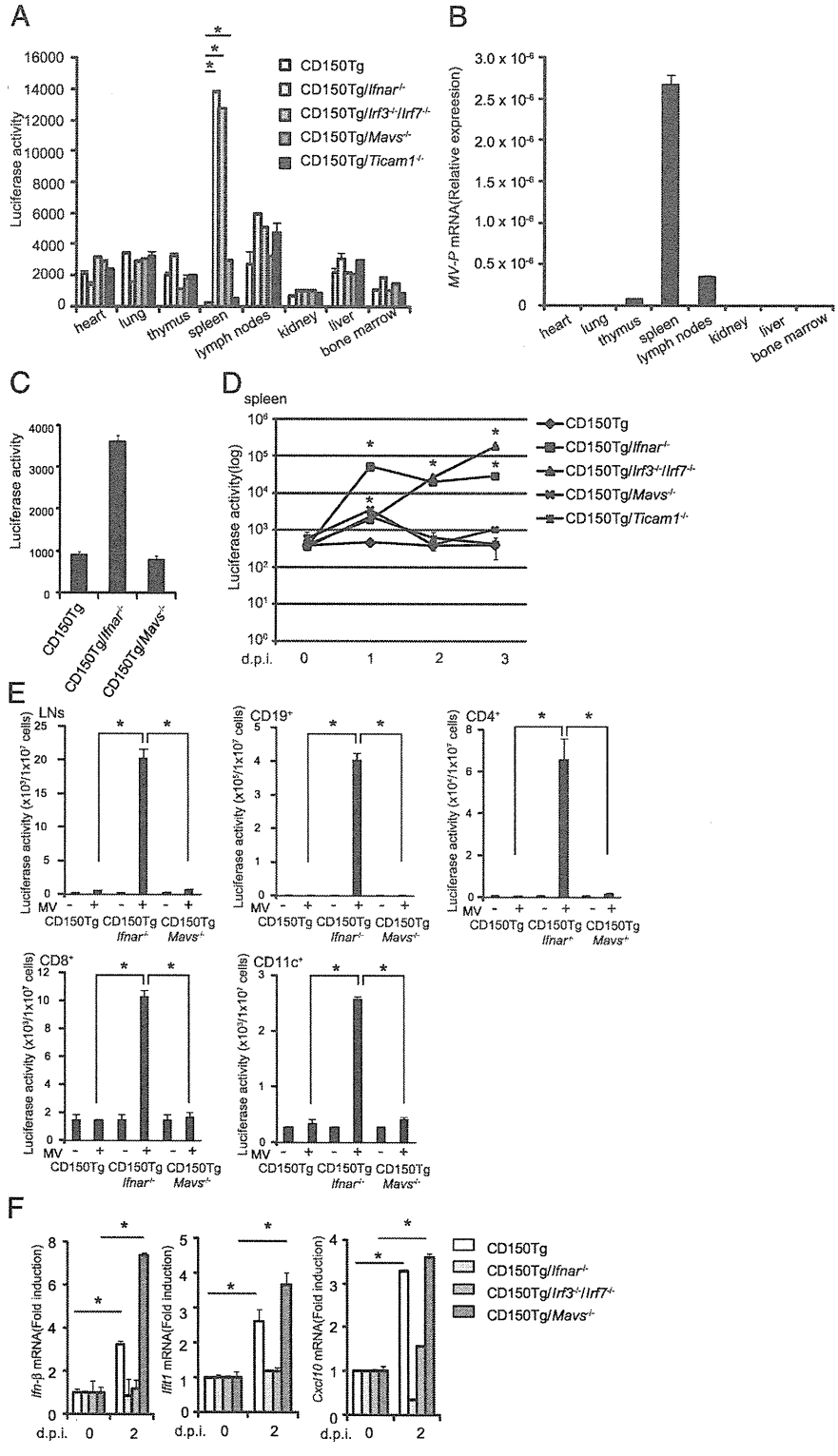

FIGURE 1. CD150Tg/*Mavs*$^{-/-}$ mice were resistant to in vivo MV infection. (**A**) CD150Tg, CD150Tg/*Ifnar*$^{-/-}$, CD150Tg/*Irf3*$^{-/-}$/*Irf7*$^{-/-}$, CD150Tg/*Mavs*$^{-/-}$, and CD150Tg/*Ticam1*$^{-/-}$ mice were infected i.p. with 1×10^6 PFU MV-luciferase. After 2 d, cells were isolated from each organ and lysed with lysis buffer for luciferase assay. The amount of protein in each lysate was determined by bicinchoninic acid assay. Luciferase activity in each lysate was measured and normalized by the amount of protein. Data are shown as luciferase activity per 1 mg of protein and means ± SD of three independent samples. *$p < 0.05$. (**B**) CD150Tg/*Ifnar*$^{-/-}$ mice were infected with MV (1×10^6 PFU). At 2 d after inoculation, total RNA was collected from the indicated tissues, and the expression level of *MV-P* mRNA in each tissue was determined by real-time PCR. *MV-P* mRNA expression is shown as expression relative to *β-actin*. Data are means ± SD of three independent samples. (**C**) CD150Tg, CD150Tg/*Ifnar*$^{-/-}$, and CD150Tg/*Mavs*$^{-/-}$ mice were intratracheally injected with MV-luciferase (8×10^5 PFU). At 3 d after inoculation, luciferase activity was measured in cells from lungs. Data are means ± SD of two independent samples. (**D**) At the indicated days post infection (d.p.i.), luciferase activity in 1×10^7 splenocytes was measured. Three mice were analyzed for each genotype. Data are representative of two independent experiments. *$p < 0.05$ versus CD150Tg. (**E**) CD150Tg, CD150Tg/*Ifnar*$^{-/-}$, and CD150Tg/*Mavs*$^{-/-}$ mice were infected i.p. with 1×10^6 PFU MV-luciferase. At 2 d.p.i., CD19$^+$, CD4$^+$, CD8$^+$, and CD11c$^+$ cells were isolated from splenocytes, using anti-CD19, anti-CD4, anti-CD8, and anti-CD11c MACS beads. Luciferase activity in CD19$^+$, CD4$^+$, CD8$^+$, and CD11c$^+$ cells, as well as LNs, was measured and normalized by the total number of cells. Data are shown as the luciferase activity per 1×10^7 cells. Data are means ± SD of three independent samples. *$p < 0.05$. (**F**) CD150Tg, CD150Tg/*Ifnar*$^{-/-}$, CD150Tg/*Irf3*$^{-/-}$/*Irf7*$^{-/-}$, and CD150Tg/*Mavs*$^{-/-}$ mice were infected i.p. with 1×10^6 PFU MV-luciferase. At 2 d.p.i., mRNA levels of *Ifn-β*, *Ifit1*, and *Cxcl10* in spleens were determined by real time-PCR. Data are means ± SD of three independent samples. *$p < 0.05$.

(Fig. 1C). However, the route of MV administration is an issue to be further investigated.

In MV-infected human epithelial cells, signals via RIG-I and MDA5 are essential for production of type I IFN (9, 10). Cells lacking the MAVS protein, a common adaptor molecule for RIG-I and MDA5, are unable to produce type I IFN in response to members of the Paramyxoviridae family (8). To investigate the in vivo role of the MAVS pathway during MV infection, we first examined whether CD150Tg/*Mavs*$^{-/-}$ mice were permissive to MV infection. Although luciferase activity in splenocytes was slightly increased in CD150Tg/*Mavs*$^{-/-}$ mice compared with CD150Tg mice 1 d after i.p. inoculation, luciferase activity in splenocytes of CD150Tg/*Mavs*$^{-/-}$ mice was decreased to the same degree as in those of CD150Tg mice a few days after inoculation (Fig. 1A, 1D, 1E). In contrast, luciferase activity in splenocytes was significantly increased in CD150Tg/*Ifnar*$^{-/-}$ and CD150Tg/*Irf3*$^{-/-}$/*Irf7*$^{-/-}$ mice compared with CD150Tg, CD150Tg/*Mavs*$^{-/-}$, or CD150Tg/*Ticam1*$^{-/-}$ mice 2 d after inoculation (Fig. 1D). We also examined luciferase activity in LNs and CD4$^+$, CD8$^+$, CD19$^+$, and CD11c$^+$ cells isolated from splenocytes of the mice. As shown in Fig. 1E, luciferase activity in these cells from MV-infected CD150Tg/*Mavs*$^{-/-}$ mice was much lower than in those from CD150Tg/*Ifnar*$^{-/-}$ mice. To investigate the reasons why CD150Tg/*Mavs*$^{-/-}$ mice were resistant to MV infection, we examined the expression level of mRNA coding antiviral protein in splenocytes (Fig. 1F). The expression of *Ifn-β* and two IFN-inducible genes, *Ifit1* and *Cxcl10*, was upregulated by MV infection in splenocytes from CD150Tg/*Mavs*$^{-/-}$ mice, but not in those from CD150Tg/*Ifnar*$^{-/-}$ and CD150Tg/*Irf3*$^{-/-}$/*Irf7*$^{-/-}$ mice (Fig. 1F). Type I IFN levels in sera were below the detection limit throughout the time course (data not shown). These data suggest that in vivo MV infection induces the expression of type I IFN and IFN-inducible genes to elicit resistance to MV infection in CD150Tg/*Mavs*$^{-/-}$. Moreover, type I IFN induction by in vivo MV infection occurs via the IRF3/IRF7-dependent and MAVS-independent pathway.

Next, we performed in vivo infection experiments using IFNAR Ab. Type I IFNR in CD150Tg/*Mavs*$^{-/-}$ mice was blocked by injecting 2.5 mg of the MAR1-5A3 mAb against IFNAR-1, 1 d before infection. This dose of Ab is reported to block antiviral effects of type I IFN in vivo (31). In MV-infected CD150Tg/*Mavs*$^{-/-}$ mice, blocking of IFNAR increased luciferase activity in LNs up to 180-fold, and in splenocytes up to 10-fold (Fig. 2A). Similarly, luciferase activity was increased up to 6-fold in CD19$^+$, 8-fold in CD4$^+$, 29-fold in CD8$^+$, and 17-fold in CD11c$^+$ cells by IFNAR blocking (Fig. 2B). These results indicate that CD150Tg/*Mavs*$^{-/-}$ mice are permissive to MV infection once IFNAR is functionally neutralized.

CD11c$^+$ DCs produce type I IFN via the MAVS-independent pathway during MV infection

To determine which cell types were responsible for type I IFN induction in MV-infected CD150Tg/*Mavs*$^{-/-}$ mice, we performed an in vitro infection assay using splenocytes. When infected with MV in vitro, the luciferase activity in B cells and T cells isolated from CD150Tg/*Mavs*$^{-/-}$ mice was comparable to activity in those from CD150Tg/*Ifnar*$^{-/-}$ mice (Fig. 3A). Treatment with anti-IFNAR Ab did not affect the infection efficiency in CD150Tg/*Mavs*$^{-/-}$ T and B cells (Fig. 3A). Unlike T and B cells, CD150Tg/*Mavs*$^{-/-}$ CD11c$^+$ DCs were not permissive to MV (Fig. 3A). These data suggest that CD11c$^+$ DCs, but not lymphocytes, are responsible for resistance to MV infection in CD150Tg/*Mavs*$^{-/-}$ mice. Because CD150Tg/*Mavs*$^{-/-}$ mice were permissive to MV in vivo when type I IFN signaling was blocked by anti-IFNAR Ab

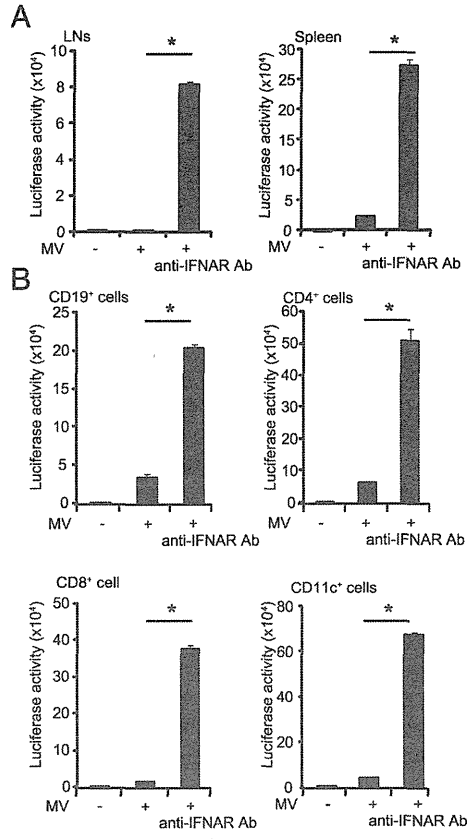

FIGURE 2. CD150Tg/*Mavs*$^{-/-}$ mice were permissive to MV after treatment with anti-IFNAR Ab in vivo. CD150Tg/*Mavs*$^{-/-}$ mice were injected i.p. with 2.5 mg of anti-IFNAR Ab at 1 d before MV-luciferase infection (1×10^7 PFU per mouse). At 2 d post infection, luciferase activity in LNs, splenocytes (**A**), and (**B**) CD19$^+$, CD4$^+$, CD8$^+$, and CD11c$^+$ cells isolated from splenocytes was measured and normalized by the total number of cells. Data are shown as the luciferase activity per 1×10^7 cells. Data are means ± SD of three independent samples. $^*p < 0.05$.

(Fig. 2A, 2B), we examined whether treatment with anti-IFNAR Ab increased the efficiency of MV infection in vitro. CD150Tg/*Mavs*$^{-/-}$ CD11c$^+$ DCs were permissive to MV in the presence of anti-IFNAR Ab (Fig. 3A). Consistent with results in Fig. 3A, type I IFN was detectable in the culture supernatant of MV-infected CD150Tg/*Mavs*$^{-/-}$ CD11c$^+$ DCs, but not of T or B cells (Fig. 3B and data not shown). Expression of *Ifn-β* and *Ifn-α4* mRNAs in CD150Tg/*Mavs*$^{-/-}$ CD11c$^+$ DCs was also upregulated within 6 h after MV infection (Fig. 3C). These data suggest that CD11c$^+$ DCs, but neither T nor B cells, mainly produce type I IFN through the MAVS-independent pathway in response to MV infection in vitro.

CD4$^+$ DCs and pDCs are responsible for MV-induced type I IFN production in CD150Tg/Mavs$^{-/-}$ *mice*

Our data indicate that type I IFN induction following the MV recognition in mouse DCs is independent of the MAVS pathway. Various types of DCs have been identified in mouse secondary lymphoid tissues, including three CD11c^{high} subsets: CD8α$^+$, CD4$^+$, and DN CD4$^-$CD8α$^-$ DCs (32), and one subset of CD11c^{low} pDCs (33). To identify the type I IFN-producing subsets, we used a cell sorter to isolate CD11c^{high} (cDCs) and CD11c^{low} pDCs from splenocytes, with purity > 98% (data not shown). CD150Tg/*Ifnar*$^{-/-}$ cDCs and pDCs were permissive to MV (Fig. 4A and 4C). In contrast, both CD150Tg/*Mavs*$^{-/-}$ cDCs and pDCs

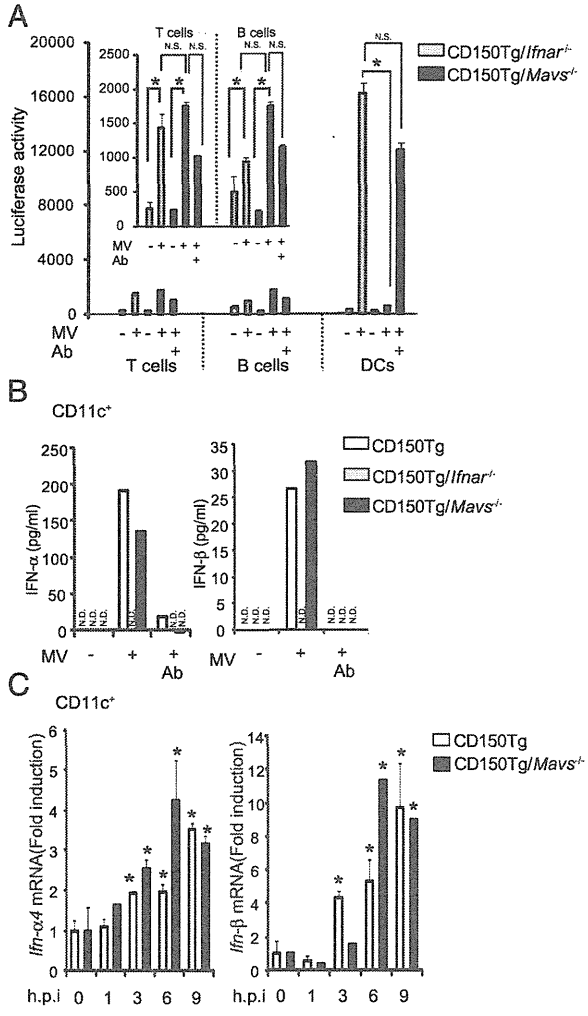

FIGURE 3. CD11c$^+$ DCs mainly produced type I IFN during MV infection in vitro. (**A**) T cells, B cells, and DCs were isolated from CD150Tg/*Ifnar*$^{-/-}$ and CD150Tg/*Mavs*$^{-/-}$ splenocytes, using MACS beads. Cells were treated with or without 10 μg/ml of anti-IFNAR Ab, then infected with mock or MV-luciferase at an MOI of 0.25. At 24 h post infection, luciferase activity was measured. Data are means ± SD of three independent samples. *$p < 0.05$. (**B**) CD11c$^+$ cells were prepared from splenocytes of CD150Tg, CD150Tg/*Ifnar*$^{-/-}$, and CD150Tg/*Mavs*$^{-/-}$ mice, using MACS beads. IFN-α and IFN-β protein production in culture supernatant of MV-infected cells (MOI = 0.25) was measured by ELISA. One of two experiments is shown. (**C**) CD11c$^+$ DCs were infected with MV (MOI of 0.25) for the indicated times, and type I IFN expression was determined by real-time PCR. Data are means ± SD of three independent samples. *A *t* test between 0 h.p.i. and the indicated time in respective mouse lines is $p < 0.05$. N.D., Not detected.

produced type I IFN (Fig. 4B, 4D) and were not permissive to MV (Fig. 4A, 4C). The resistance to MV infection was abolished by neutralizing type I IFNR with anti-IFNAR Ab (Fig. 4A, 4C). These data indicate that, like CD11c$^+$ DCs, CD150Tg/*Mavs*$^{-/-}$ pDCs and cDCs were barely permissive to MV because of the type I IFN production.

For more detailed study on the type I IFN-producing subsets, we further separated cDCs into CD8α$^+$, CD4$^+$, and DN DCs, using MACS beads. The purity of these subsets was > 90% (data not shown). *Ifn-β* mRNA was not induced in CD150Tg/*Mavs*$^{-/-}$ CD8α$^+$ DCs or DN DCs in response to MV infection (Fig. 5A, 5B). However, MV infection induced expression of *Ifn-β* mRNA in CD4$^+$ DCs from CD150Tg/*Mavs*$^{-/-}$ mice (Fig. 5C). Different from CD150Tg/*Mavs*$^{-/-}$ DCs, CD150Tg CD8α$^+$ and DN DCs expressed *Ifn-β* mRNA in response to MV infection (Fig. 5A, 5B). These data indicate that the expression of *Ifn-β* mRNA induced by MV infection is MAVS dependent in CD8α$^+$ DCs and DNs, but MAVS independent in CD4$^+$ DCs.

The MyD88-dependent pathway is essential for MV-induced type I IFN production in pDCs and CD4$^+$ DCs under MAVS deficiency

Next, we tried to identify the signaling pathway involved in type I IFN induction during MV infection. pDCs and CD4$^+$ DCs express TLR7 as a sensor for single-stranded RNA (34, 35). Recognition of single-stranded RNA through the TLR7-MyD88 pathway induces type I IFN expression in human and mouse pDCs (36–38). Therefore, we examined whether the TLR7-MyD88 pathway participated in the host defense during MV infection in mouse DCs. First, we analyzed the expression of TLR7 in pDCs and CD4$^+$ DCs. As reported in previous studies (34, 35), we were able to detect the expression of TLR7 at both mRNA and protein levels (Supplemental Fig. 2). RNA interference cannot be used in primary pDCs because the RNA molecules induce type I IFN expression (39); therefore, we used a peptide that is fused to an antennapedia-derived cell permeant motif and inhibits MyD88 homodimerization by binding to the MyD88 TIR domain (40). pDCs from wild-type mice were cultured for 6 h in the presence of the MyD88 inhibitory peptide or the control peptide and activated with R837, a TLR7 ligand, for 24 h. The control peptide marginally affected IFN-β secretion induced by R837, and the MyD88 inhibitory peptide at 50 μM significantly reduced IFN-β production induced by R837 (Supplemental Fig. 3A). To evaluate the effects of the inhibitory peptide on cell viability, we counted the number of live cells using trypan blue staining (Supplemental Fig. 3B). Although stimulation with R837 partially induced cell death (41.3% ± 5.4%), cell viability was not changed by the addition of the inhibitory peptide at 50 μM (Supplemental Fig. 3B). MyD88 inhibitory peptide has no effects on polyinosinic/polycytidylic acid–induced IFN-β production in CD11c$^+$ DCs (Supplemental Fig. 3C). Next, we tested the effect of MyD88 inhibitory peptide on permissiveness and type I IFN production in MV-infected pDCs from CD150Tg/*Mavs*$^{-/-}$ mice. Although CD150Tg/*Mavs*$^{-/-}$ pDCs were not permissive to MV in the presence of control peptide, infection efficiency was increased 4-fold by treatment with MyD88 inhibitory peptide (Fig. 6A). As with pDCs, the infection efficiency of CD150Tg/*Mavs*$^{-/-}$ CD11c$^+$ DCs increased 3-fold by MyD88 inhibitory peptide treatment (Fig. 6B). When CD150Tg/*Mavs*$^{-/-}$ CD11c$^+$ DCs, CD4$^+$ DCs, and pDCs were pretreated with MyD88 inhibitory peptide, they did not induce type I IFN mRNA after MV infection (Fig. 6C–E). These data suggest that the MyD88 pathway is responsible for MV-induced type I IFN production in DCs under MAVS deficiency. To confirm that the MyD88 pathway is involved in type I IFN induction in MV-infected DCs, CD150Tg/*Myd88*$^{-/-}$ pDCs were infected with MV in vitro. *Ifn-β* mRNA expression was not induced in MV-infected CD150Tg/*Myd88*$^{-/-}$ pDCs (Fig. 6F).

Discussion

This study demonstrated that CD150Tg/*Mavs*$^{-/-}$ mice were not susceptible to MV infection in vivo (Fig. 1). This is an unexpected result because many reports have highlighted the important role of the RIG-I/MDA5-MAVS pathway in type I IFN production in MV-infected cells as a means to suppress MV replication. Ultimately, the MyD88 signal, rather than the MAVS signal, serves as a critical inducer of primary type I IFN for cell protection against

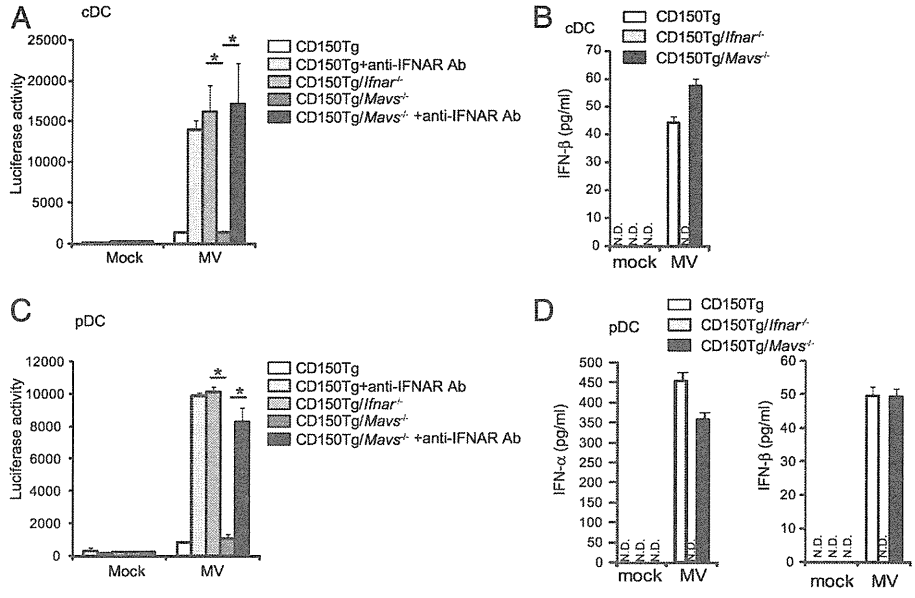

FIGURE 4. CD150Tg/*Mavs*$^{-/-}$ pDCs produced type I IFN in response to MV infection. The cDCs (**A**, **B**) or pDCs (**C**, **D**) isolated from CD150Tg, CD150Tg/*Ifnar*$^{-/-}$, or CD150Tg/*Mavs*$^{-/-}$ splenocytes were infected by MV (MOI of 0.25). At 24 h post infection, luciferase activity was measured (A, C). Production of type I IFN in culture supernatant was measured by ELISA (B, D). Data are means ± SD of three independent samples. N.D., Not detected.

MV replication in a mouse model. This finding would be a novel feature of MV, a negative single-stranded RNA virus, and has reminded us that cell-level studies on host innate immunity in coping with infection cannot always predict critical virus-sensing factors in whole-animal studies.

Because blockage of type I IFNR function resulted in permissiveness of CD150Tg/*Mavs*$^{-/-}$ mice to MV, MAVS-independent type I IFN induction protects neighboring cells (that express IFNAR) from MV infection (Fig. 2). Among the cell subsets tested, only pDCs and CD4$^+$ DCs from CD150Tg/*Mavs*$^{-/-}$ produced type I IFN after MV infection (Figs. 3–5). Treatment with inhibitory peptide for MyD88 drastically decreased type I IFN expression in CD150Tg/*Mavs*$^{-/-}$ DCs and rendered these cells MV permissive to MV (Fig. 6). These data indicate that the MyD88 pathway is involved in type I IFN induction in MV-infected pDCs and CD4$^+$ DCs under a MAVS-deficient state. The results were confirmed with CD150/*Myd88*$^{-/-}$ mice (Fig. 6F). In this context, the MyD88 pathway plays a primary role in the initial phase of MV protection in vivo. However, CD150Tg/*Myd88*$^{-/-}$ mice were not permissive to MV in vivo (data not shown), suggesting that not only MyD88 in pDCs/CD4$^+$ DCs but also MAVS in other cells contributes to the protection against systemic infection by MV. Because the MyD88 pathway participates in the initial type I IFN induction in pDCs, only a very weak but significant luciferase activity was detected in the spleen of CD150Tg/*Mavs*$^{-/-}$ mice at day 1 after inoculation (Fig. 1C). Moreover, CD8α$^+$ DCs and DN DCs from CD150Tg/*Mavs*$^{-/-}$ mice could not induce *Ifn-β* mRNA expression in response to MV infection in vitro (Fig. 5). These results suggest that the MAVS pathway also participates in host defense against MV infection as an alternative pathway in splenic DCs, at least in these experimental conditions.

Another target cell of MV infection in nonhuman primates is the AM (18). AMs in the CD150Tg/*Ifnar*$^{-/-}$ mouse model are also permissive to MV infection (17). AMs derived from CD150Tg/*Mavs*$^{-/-}$ mice were permissive to MV infection in vitro (data not shown). This result is consistent with a previous report indicating that the RLR-MAVS pathway is predominantly used for type I IFN induction in virus-infected AMs (41). However, intratracheal inoculation with MV in CD150Tg/*Mavs*$^{-/-}$ mice resulted in a lower luciferase activity in AMs from CD150Tg/*Mavs*$^{-/-}$ mice than in those from CD150Tg/*Ifnar*$^{-/-}$ mice (data not shown), similar to the results from i.p. inoculation. These data indicate that a cell population other than AMs produces type I IFN in MV-infected lungs. In this case, pDCs in lung might act as IFN-producing cells, because pDCs in lung are reported to produce type I IFN and act as immune system defenders against infection (41). Taken together, the recognition pathways for MV to induce type I IFN differ among cell types. Existence of the several alternative pathways might engage the protection from systemic MV infection (Supplemental Fig. 4).

In CD8α$^-$ DCs and pDCs, the TLR-MyD88 pathway is preferentially used to induce type I IFN in response to infections. TLR7, a sensor for viral RNA, is known to be expressed specifically in these DC subsets (34, 35) (Supplemental Fig. 2). The restricted expression pattern of TLR7 seems to reflect the ability of CD4$^+$ DCs and pDCs to produce type I IFN in MV-infected CD150Tg/*Mavs*$^{-/-}$. Therefore, TLR7 may be one of the candidate receptors for recognition of MV RNA. Because viral RNA is recognized mainly through the RLR-MAVS pathway in CD4$^+$ DCs at steady state (35), it would be difficult to examine the role of the TLR7-MyD88 pathway in CD4$^+$ DCs during viral infection in WT mice. Thus, our assay system using CD150Tg mice crossed with given knockout mice is a powerful tool to investigate the signaling pathway for host defense against MV infection.

Previous studies were mainly done using bone marrow–derived DCs (BMDCs) to analyze the immunosuppressive effects of MV in a mouse model (16, 42, 43). However, BMDCs from CD150Tg/*Mavs*$^{-/-}$ mice completely lacked the ability to produce type I IFN in response to MV infection. In contrast to the results in splenic DCs (44). Because the expression profile of pattern-recognition receptors in BMDCs was different from the profile in splenic DCs (34, 35, 45), it is reasonable to think that each cell type has its own unique type I IFN induction pathway in response to viral infection. Therefore, further investigations on immunosuppression and immunopromotion of MV in infected DCs should be performed using splenic DCs, taking into consideration the properties of resident DCs.

In this study, we used recombinant MV-luciferase that expresses the reporter *Renilla* luciferase from the first gene position of MV genome (29). The MV-luciferase is suitable to evaluate the efficiency of infection in vivo and in vitro correctly because the assay

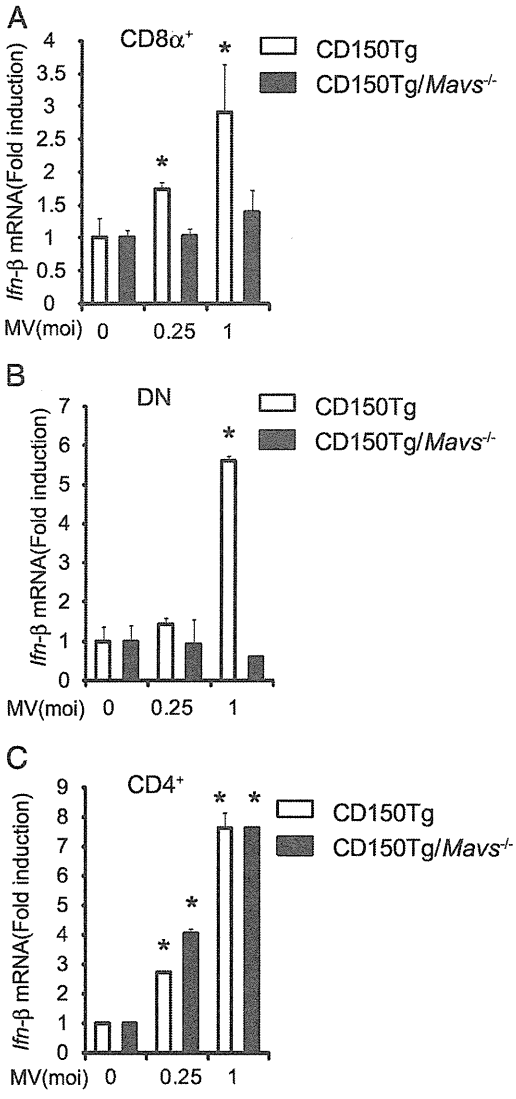

FIGURE 5. MV-infected CD150Tg/*Mavs*$^{-/-}$ CD4$^+$ DCs expressed type I IFN mRNA. CD8α$^+$ DCs (**A**), DN DCs (**B**), and CD4$^+$ DCs (**C**) were isolated by MACS beads. Cells were infected with MV (MOI of 0.25 or 1.0) for 9 h, and levels of *Ifn-β* mRNA were measured by real-time PCR. Data are means ± SD of three independent samples. *A *t* test between 0 h. p.i. and the indicate time in respective mouse line is $p < 0.05$.

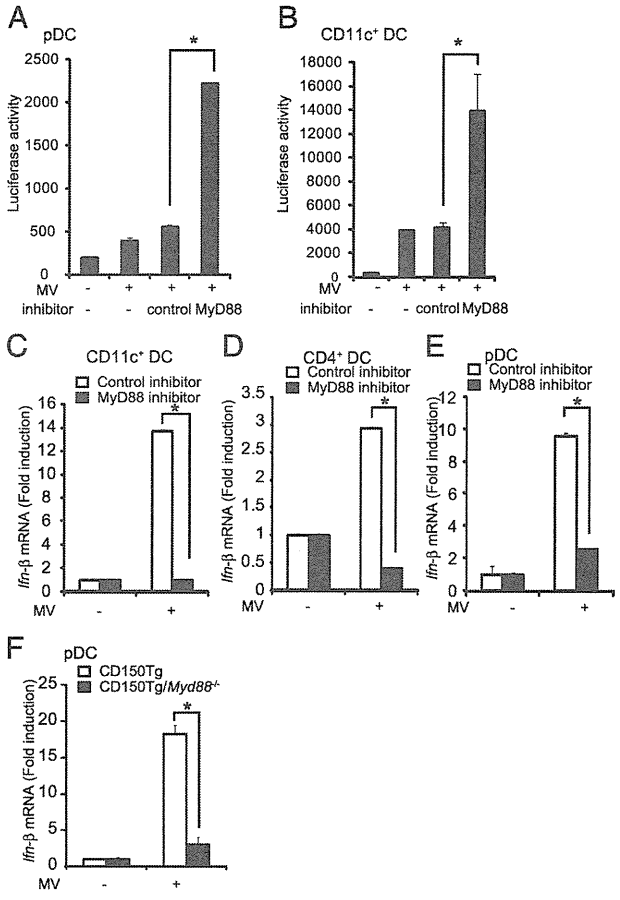

FIGURE 6. The MyD88 pathway is responsible for MV-induced type I IFN induction in CD150Tg/*Mavs*$^{-/-}$ DCs. (**A**) pDCs were isolated by FACS or (**B**) CD11c$^+$ DCs were isolated by MACS beads from CD150Tg/*Mavs*$^{-/-}$ splenocytes. Cells were treated with 50 μM of the control peptide or 50 μM of the MyD88 inhibitory peptide for 6 h and then infected with MV (MOI of 0.25). After 18 h, luciferase activity was measured. Data are means ± SD of three independent samples. CD150Tg/*Mavs*$^{-/-}$ CD11c$^+$ DCs (**C**), CD4$^+$ DCs (**D**), and pDCs (**E**) were pretreated with 50 μM control peptide or 50 μM MyD88 inhibitory peptide for 6 h following infection with MV (MOI of 0.25) for 9 h. Expression levels of *Ifn-β* mRNA were measured by real-time PCR. Expression levels of data are means ± SD of three independent samples. (**F**) *Ifn-β* mRNA expression in MV-infected CD150Tg and CD150Tg/*Myd88*$^{-/-}$ pDCs. pDCs were infected with MV (MOI = 0.25) for 9 h. Expression levels of *Ifn-β* mRNA were measured by real-time PCR. Expression levels of data are means ± SD of three independent samples. *$p < 0.05$.

system worked well using the CD150Tg/*Ifnar*$^{-/-}$ mouse model. Luciferase activity and MV-P mRNA in CD150Tg/*Ifnar*$^{-/-}$ was significantly increased compared with CD150Tg mice during infection (Fig. 1A, 1B and data not shown). Luciferase activity obtained from MV-infected Vero/CD150 cells was correlated with viral titer in culture supernatant from MV-infected cells (data not shown). Recombinant MV strains expressing a foreign gene from a first gene position of the MV genome were used in several groups for in vivo infection assay without any problem (17, 18, 24). However, the infection efficiency of recombinant *Morbillivirus* expressing a foreign gene from position one is reported to be attenuated in vivo (46), which is well reflected in the relatively low virus titer observed in the spleen from CD150Tg mice infected with MV-luciferase.

In mouse models, the route of MV inoculation does not always reflect the natural infection route in human MV infection. Our results obtained from experiments using the i.p. infection model also may not faithfully reflect the process of natural MV infection involving epithelial cells in humans. However, as described above, intratracheal and i.p. administration gave rise to similar results in MV infection. This issue may reflect the viral strategy of targeting myeloid cells for initial propagation. Injected MV reaches DCs or macrophages without affecting other bystander cells in any route of MV administration. However, this is not the case in other virus species with different target cells for initial infection.

We conclude that MyD88-dependent type I IFN production in CD4$^+$ DCs and pDCs results in initial protection against MV; thereafter, the produced type I IFN induces an antiviral state in the neighboring cells, expressing IFNAR in the mouse model.

Acknowledgments

We thank Drs. T. Taniguchi (University of Tokyo, Tokyo, Japan) and S. Akira (Osaka University, Osaka, Japan) for providing *Irf3*$^{-/-}$/*Irf7*$^{-/-}$ and *Myd88*$^{-/-}$ mice, respectively, for this study, and Dr. Y. Yanagi (Kyushu University, Fukuoka, Japan) for providing MV-luciferase.

Disclosures

The authors have no financial conflicts of interest.

References

1. Honda, K., A. Takaoka, and T. Taniguchi. 2006. Type I interferon [corrected] gene induction by the interferon regulatory factor family of transcription factors. *Immunity* 25: 349–360.
2. Yoneyama, M., K. Onomoto, and T. Fujita. 2008. Cytoplasmic recognition of RNA. *Adv. Drug Deliv. Rev.* 60: 841–846.
3. Takeuchi, O., and S. Akira. 2009. Innate immunity to virus infection. *Immunol. Rev.* 227: 75–86.
4. Yamamoto, M., S. Sato, K. Mori, K. Hoshino, O. Takeuchi, K. Takeda, and S. Akira. 2002. Cutting edge: a novel Toll/IL-1 receptor domain-containing adapter that preferentially activates the IFN-beta promoter in the Toll-like receptor signaling. *J. Immunol.* 169: 6668–6672.
5. Oshiumi, H., M. Matsumoto, K. Funami, T. Akazawa, and T. Seya. 2003. TICAM-1, an adaptor molecule that participates in Toll-like receptor 3-mediated interferon-beta induction. *Nat. Immunol.* 4: 161–167.
6. Kawai, T., K. Takahashi, S. Sato, C. Coban, H. Kumar, H. Kato, K. J. Ishii, O. Takeuchi, and S. Akira. 2005. IPS-1, an adaptor triggering RIG-I- and Mda5-mediated type I interferon induction. *Nat. Immunol.* 6: 981–988.
7. Yamamoto, M., S. Sato, H. Hemmi, K. Hoshino, T. Kaisho, H. Sanjo, O. Takeuchi, M. Sugiyama, M. Okabe, K. Takeda, and S. Akira. 2003. Role of adaptor TRIF in the MyD88-independent toll-like receptor signaling pathway. *Science* 301: 640–643.
8. Kumar, H., T. Kawai, H. Kato, S. Sato, K. Takahashi, C. Coban, M. Yamamoto, S. Uematsu, K. J. Ishii, O. Takeuchi, and S. Akira. 2006. Essential role of IPS-1 in innate immune responses against RNA viruses. *J. Exp. Med.* 203: 1795–1803.
9. Ikegame, S., M. Takeda, S. Ohno, Y. Nakatsu, Y. Nakanishi, and Y. Yanagi. 2010. Both RIG-I and MDA5 RNA helicases contribute to the induction of alpha/beta interferon in measles virus-infected human cells. *J. Virol.* 84: 372–379.
10. Berghäll, H., J. Sirén, D. Sarkar, I. Julkunen, P. B. Fisher, R. Vainionpää, and S. Matikainen. 2006. The interferon-inducible RNA helicase, mda-5, is involved in measles virus-induced expression of antiviral cytokines. *Microbes Infect.* 8: 2138–2144.
11. Griffin, D. E. 1995. Immune responses during measles virus infection. *Curr. Top. Microbiol. Immunol.* 191: 117–134.
12. Tatsuo, H., N. Ono, K. Tanaka, and Y. Yanagi. 2000. SLAM (CDw150) is a cellular receptor for measles virus. *Nature* 406: 893–897.
13. Mühlebach, M. D., M. Mateo, P. L. Sinn, S. Prüfer, K. M. Uhlig, V. H. Leonard, C. K. Navaratnarajah, M. Frenzke, X. X. Wong, B. Sawatsky, et al. 2011. Adherens junction protein nectin-4 is the epithelial receptor for measles virus. *Nature* 480: 530–533.
14. Noyce, R. S., D. G. Bondre, M. N. Ha, L. T. Lin, G. Sisson, M. S. Tsao, and C. D. Richardson. 2011. Tumor cell marker PVRL4 (nectin 4) is an epithelial cell receptor for measles virus. *PLoS Pathog.* 7: e1002240.
15. Delpeut, S., R. S. Noyce, R. W. Siu, and C. D. Richardson. 2012. Host factors and measles virus replication. *Curr Opin Virol* 2: 773–783.
16. Shingai, M., N. Inoue, T. Okuno, M. Okabe, T. Akazawa, Y. Miyamoto, M. Ayata, K. Honda, M. Kurita-Taniguchi, M. Matsumoto, et al. 2005. Wild-type measles virus infection in human CD46/CD150-transgenic mice: CD11c-positive dendritic cells establish systemic viral infection. *J. Immunol.* 175: 3252–3261.
17. Ferreira, C. S., M. Frenzke, V. H. Leonard, G. G. Welstead, C. D. Richardson, and R. Cattaneo. 2010. Measles virus infection of alveolar macrophages and dendritic cells precedes spread to lymphatic organs in transgenic mice expressing human signaling lymphocytic activation molecule (SLAM, CD150). *J. Virol.* 84: 3033–3042.
18. Lemon, K., R. D. de Vries, A. W. Mesman, S. McQuaid, G. van Amerongen, S. Yüksel, M. Ludlow, L. J. Rennick, T. Kuiken, B. K. Rima, et al. 2011. Early target cells of measles virus after aerosol infection of non-human primates. *PLoS Pathog.* 7: e1001263.
19. Mesman, A. W., R. D. de Vries, S. McQuaid, W. P. Duprex, R. L. de Swart, and T. B. Geijtenbeek. 2012. A prominent role for DC-SIGN+ dendritic cells in initiation and dissemination of measles virus infection in non-human primates. *PLoS ONE* 7: e49573.
20. Schneider-Schaulies, S., I. M. Klagge, and V. ter Meulen. 2003. Dendritic cells and measles virus infection. *Curr. Top. Microbiol. Immunol.* 276: 77–101.
21. Servet-Delprat, C., P. O. Vidalain, H. Valentin, and C. Rabourdin-Combe. 2003. Measles virus and dendritic cell functions: how specific response cohabits with immunosuppression. *Curr. Top. Microbiol. Immunol.* 276: 103–123.
22. Welstead, G. G., C. Iorio, R. Draker, J. Bayani, J. Squire, S. Vongpunsawad, R. Cattaneo, and C. D. Richardson. 2005. Measles virus replication in lymphatic cells and organs of CD150 (SLAM) transgenic mice. *Proc. Natl. Acad. Sci. USA* 102: 16415–16420.
23. Sellin, C. I., N. Davoust, V. Guillaume, D. Baas, M. F. Belin, R. Buckland, T. F. Wild, and B. Horvat. 2006. High pathogenicity of wild-type measles virus infection in CD150 (SLAM) transgenic mice. *J. Virol.* 80: 6420–6429.
24. Ohno, S., N. Ono, F. Seki, M. Takeda, S. Kura, T. Tsuzuki, and Y. Yanagi. 2007. Measles virus infection of SLAM (CD150) knockin mice reproduces tropism and immunosuppression in human infection. *J. Virol.* 81: 1650–1659.
25. Akazawa, T., T. Ebihara, M. Okuno, Y. Okuda, M. Shingai, K. Tsujimura, T. Takahashi, M. Ikawa, M. Okabe, N. Inoue, et al. 2007. Antitumor NK activation induced by the Toll-like receptor 3-TICAM-1 (TRIF) pathway in myeloid dendritic cells. *Proc. Natl. Acad. Sci. USA* 104: 252–257.
26. Oshiumi, H., M. Okamoto, K. Fujii, T. Kawanishi, M. Matsumoto, S. Koike, and T. Seya. 2011. The TLR3/TICAM-1 pathway is mandatory for innate immune responses to poliovirus infection. *J. Immunol.* 187: 5320–5327.
27. Kobune, F., H. Sakata, and A. Sugiura. 1990. Marmoset lymphoblastoid cells as a sensitive host for isolation of measles virus. *J. Virol.* 64: 700–705.
28. Takeda, M., K. Takeuchi, N. Miyajima, F. Kobune, Y. Ami, N. Nagata, Y. Suzaki, Y. Nagai, and M. Tashiro. 2000. Recovery of pathogenic measles virus from cloned cDNA. *J. Virol.* 74: 6643–6647.
29. Takeda, M., M. Tahara, T. Hashiguchi, T. A. Sato, F. Jinnouchi, S. Ueki, S. Ohno, and Y. Yanagi. 2007. A human lung carcinoma cell line supports efficient measles virus growth and syncytium formation via a SLAM- and CD46-independent mechanism. *J. Virol.* 81: 12091–12096.
30. Shingai, M., T. Ebihara, N. A. Begum, A. Kato, T. Honma, K. Matsumoto, H. Saito, H. Ogura, M. Matsumoto, and T. Seya. 2007. Differential type I IFN-inducing abilities of wild-type versus vaccine strains of measles virus. *J. Immunol.* 179: 6123–6133.
31. Sheehan, K. C., K. S. Lai, G. P. Dunn, A. T. Bruce, M. S. Diamond, J. D. Heutel, C. Dungo-Arthur, J. A. Carrero, J. M. White, P. J. Hertzog, and R. D. Schreiber. 2006. Blocking monoclonal antibodies specific for mouse IFN-alpha/beta receptor subunit 1 (IFNAR-1) from mice immunized by in vivo hydrodynamic transfection. *J. Interferon Cytokine Res.* 26: 804–819.
32. Vremec, D., J. Pooley, H. Hochrein, L. Wu, and K. Shortman. 2000. CD4 and CD8 expression by dendritic cell subtypes in mouse thymus and spleen. *J. Immunol.* 164: 2978–2986.
33. Asselin-Paturel, C., A. Boonstra, M. Dalod, I. Durand, N. Yessaad, C. Dezutter-Dambuyant, A. Vicari, A. O'Garra, C. Biron, F. Brière, and G. Trinchieri. 2001. Mouse type I IFN-producing cells are immature APCs with plasmacytoid morphology. *Nat. Immunol.* 2: 1144–1150.
34. Edwards, A. D., S. S. Diebold, E. M. Slack, H. Tomizawa, H. Hemmi, T. Kaisho, S. Akira, and C. Reis e Sousa. 2003. Toll-like receptor expression in murine DC subsets: lack of TLR7 expression by CD8 alpha+ DC correlates with unresponsiveness to imidazoquinolines. *Eur. J. Immunol.* 33: 827–833.
35. Luber, C. A., J. Cox, H. Lauterbach, B. Fancke, M. Selbach, J. Tschopp, S. Akira, M. Wiegand, H. Hochrein, M. O'Keeffe, and M. Mann. 2010. Quantitative proteomics reveals subset-specific viral recognition in dendritic cells. *Immunity* 32: 279–289.
36. Hemmi, H., T. Kaisho, O. Takeuchi, S. Sato, H. Sanjo, K. Hoshino, T. Horiuchi, H. Tomizawa, K. Takeda, and S. Akira. 2002. Small anti-viral compounds activate immune cells via the TLR7 MyD88-dependent signaling pathway. *Nat. Immunol.* 3: 196–200.
37. Heil, F., H. Hemmi, H. Hochrein, F. Ampenberger, C. Kirschning, S. Akira, G. Lipford, H. Wagner, and S. Bauer. 2004. Species-specific recognition of single-stranded RNA via toll-like receptor 7 and 8. *Science* 303: 1526–1529.
38. Diebold, S. S., T. Kaisho, H. Hemmi, S. Akira, and C. Reis e Sousa. 2004. Innate antiviral responses by means of TLR7-mediated recognition of single-stranded RNA. *Science* 303: 1529–1531.
39. Hornung, V., M. Guenthner-Biller, C. Bourquin, A. Ablasser, M. Schlee, S. Uematsu, A. Noronha, M. Manoharan, S. Akira, A. de Fougerolles, et al. 2005. Sequence-specific potent induction of IFN-alpha by short interfering RNA in plasmacytoid dendritic cells through TLR7. *Nat. Med.* 11: 263–270.
40. Loiarro, M., C. Sette, G. Gallo, A. Ciacci, N. Fantò, D. Mastroianni, P. Carminati, and V. Ruggiero. 2005. Peptide-mediated interference of TIR domain dimerization in MyD88 inhibits interleukin-1-dependent activation of NF-kappaB. *J. Biol. Chem.* 280: 15809–15814.
41. Kumagai, Y., O. Takeuchi, H. Kato, H. Kumar, K. Matsui, E. Morii, K. Aozasa, T. Kawai, and S. Akira. 2007. Alveolar macrophages are the primary interferon-alpha producer in pulmonary infection with RNA viruses. *Immunity* 27: 240–252.
42. Hahm, B., N. Arbour, and M. B. Oldstone. 2004. Measles virus interacts with human SLAM receptor on dendritic cells to cause immunosuppression. *Virology* 323: 292–302.
43. Koga, R., S. Ohno, S. Ikegame, and Y. Yanagi. 2010. Measles virus-induced immunosuppression in SLAM knock-in mice. *J. Virol.* 84: 5360–5367.
44. Takaki, H., K. Honda, K. Atarashi, F. Kobayashi, T. Ebihara, H. Oshiumi, M. Matsumoto, M. Shingai, and T. Seya. 2013. MAVS-dependent IRF3/IRF7 bypass of interferon β-induction restricts the response to measles infection in CD150Tg mouse bone marrow-derived dendritic cells. *Molec. Immunol.* In press.
45. Datta, S. K., V. Redecke, K. R. Prilliman, K. Takabayashi, M. Corr, T. Tallant, J. DiDonato, R. Dziarski, S. Akira, S. P. Schoenberger, and E. Raz. 2003. A subset of Toll-like receptor ligands induces cross-presentation by bone marrow-derived dendritic cells. *J. Immunol.* 170: 4102–4110.
46. von Messling, V., D. Milosevic, and R. Cattaneo. 2004. Tropism illuminated: lymphocyte-based pathways blazed by lethal morbillivirus through the host immune system. *Proc. Natl. Acad. Sci. USA* 101: 14216–14221.

A Distinct Role of Riplet-Mediated K63-Linked Polyubiquitination of the RIG-I Repressor Domain in Human Antiviral Innate Immune Responses

Hiroyuki Oshiumi*, Moeko Miyashita¤, Misako Matsumoto, Tsukasa Seya

Department of Microbiology and Immunology, Graduate School of Medicine, Hokkaido University, Kita-ku, Sapporo, Japan

Abstract

The innate immune system is essential for controlling viral infections, but several viruses have evolved strategies to escape innate immunity. RIG-I is a cytoplasmic viral RNA sensor that triggers the signal to induce type I interferon production in response to viral infection. RIG-I activation is regulated by the K63-linked polyubiquitin chain mediated by Riplet and TRIM25 ubiquitin ligases. TRIM25 is required for RIG-I oligomerization and interaction with the IPS-1 adaptor molecule. A knockout study revealed that Riplet was essential for RIG-I activation. However the molecular mechanism underlying RIG-I activation by Riplet remains unclear, and the functional differences between Riplet and TRIM25 are also unknown. A genetic study and a pull-down assay indicated that Riplet was dispensable for RIG-I RNA binding activity but required for TRIM25 to activate RIG-I. Mutational analysis demonstrated that Lys-788 within the RIG-I repressor domain was critical for Riplet-mediated K63-linked polyubiquitination and that Riplet was required for the release of RIG-I autorepression of its N-terminal CARDs, which leads to the association of RIG-I with TRIM25 ubiquitin ligase and TBK1 protein kinase. Our data indicate that Riplet is a prerequisite for TRIM25 to activate RIG-I signaling. We investigated the biological importance of this mechanism in human cells and found that hepatitis C virus (HCV) abrogated this mechanism. Interestingly, HCV NS3-4A proteases targeted the Riplet protein and abrogated endogenous RIG-I polyubiquitination and association with TRIM25 and TBK1, emphasizing the biological importance of this mechanism in human antiviral innate immunity. In conclusion, our results establish that Riplet-mediated K63-linked polyubiquitination released RIG-I RD autorepression, which allowed the access of positive factors to the RIG-I protein.

Citation: Oshiumi H, Miyashita M, Matsumoto M, Seya T (2013) A Distinct Role of Riplet-Mediated K63-Linked Polyubiquitination of the RIG-I Repressor Domain in Human Antiviral Innate Immune Responses. PLoS Pathog 9(8): e1003533. doi:10.1371/journal.ppat.1003533

Editor: Michael Gale Jr, University of Washington, United States of America

Received January 30, 2013; **Accepted** June 17, 2013; **Published** August 8, 2013

Funding: This work was supported in part by a grant-in-aid from the Ministry of Education, Science and Culture of Japan, and the Ministry of Health Labour, and Welfare of Japan, Kato Memorial Bioscience Foundation. The funders had no role in study design, data collection and analysis, decision to publish, or preparation of the manuscript.

Competing Interests: The authors have declared that no competing interests exist.

* E-mail: oshiumi@med.hokudai.ac.jp

¤ Current address: Hokkaido Pharmaceutical University School of Pharmacy, Katsuraoka-cho, Otaru, Hokkaido, Japan.

Introduction

The innate immune system is essential for controlling virus infections, and several viruses have evolved strategies to evade host innate immune responses. Cytoplasmic viral RNA is recognized by RIG-I-like receptors, including RIG-I and MDA5 [1,2]. The RIG-I protein comprises N-terminal Caspase Activation and Recruitment Domains (CARDs), a central RNA helicase domain, and a C-terminal Repressor domain (RD) [3]. RD consists of C-terminal RNA binding domain (CTD) and a bridging domain between CTD and helicase [4]. RIG-I CARDs are essential for triggering the signal that induces type I interferon (IFN). In resting cells, RIG-I RD represses its CARDs signaling [3]. After viral infection, RIG-I RD recognizes 5′-triphosphate double-stranded RNA (dsRNA), which results in a conformational change in the RIG-I protein [3]. This conformational change leads to the release of RD autorepression of CARDs, after which CARDs associate with an IPS-1 adaptor molecule (also called MAVS, Cardif, and VISA) localized at the outer membrane of mitochondria [3,5,6,7,8]. IPS-1 activates downstream factors such as TBK1, IKK-ε, and NEMO [9,10,11]. NEMO forms a complex with TBK1 and IKK-ε and has a polyubiquitin binding region [12]. These protein kinases are essential for activating transcription factors such as IRF-3 to induce type I IFN production [13].

Several ubiquitin ligases are involved in regulating the RIG-I-dependent pathway, and RIG-I itself is regulated by ubiquitin chains [14]. Gack MU and colleagues firstly reported that TRIM25 ubiquitin ligase mediates K63-linked polyubiquitination of RIG-I N-terminal CARDs, which results in RIG-I activation [15]. Other groups also detected a RIG-I-anchored polyubiquitin chain after ligand stimulation or viral infection [16,17]. It was recently demonstrated that an unanchored polyubiquitin chain but not ubiquitination is essential for RIG-I activation [18,19]. However, RIG-I anchored K63-linked polyubiquitin chains are detected after viral infection [15,20].

Another E3 ubiquitin ligase, Riplet, binds RIG-I RD and mediates the K63-linked polyubiquitination of RIG-I RD [21]. In contrast, Chen DY and colleagues reported that Riplet (also called Reul) ubiquitinated RIG-I CARDs [22]. A study that used Riplet knockout mice showed that mouse Riplet is essential for RIG-I-

Author Summary

The cytoplasmic viral RNA sensor RIG-I recognizes various types of pathogenic viruses and evokes innate immune responses, whereas several viruses have evolved strategies to escape the host innate immune responses. RIG-I triggers a signal to induce type I interferon and inflammatory cytokines. RIG-I activation is regulated by K63-linked polyubiquitin chains mediated by the ubiquitin ligases TRIM25 and Riplet; however, the functional difference between the two ubiquitin ligases remains unclear, and the molecular mechanism underlying Riplet-mediated RIG-I activation is unknown. We revealed sequential roles of the two ubiquitin ligases during RIG-I activation and found that Riplet-mediated polyubiquitination of the RIG-I repressor domain released RIG-I autorepression of its N-terminal CARDs responsible for triggering the signal, which resulted in an association with TRIM25 ubiquitin ligase and TBK1 protein kinase. Interestingly, we found that this mechanism was targeted by hepatitis C virus, which is a major cause of hepatocellular carcinoma. This result emphasizes the vital role of Riplet-mediated release of RIG-I RD autorepression in antiviral responses. Our results establish that Riplet releases RIG-I RD autorepression and demonstrated the biological significance of this mechanism in human innate immune responses.

mediated type I IFN production in response to vesicular stomatitis virus (VSV), Flu, and Sendai virus (SeV) infections [23]. However, the functional difference between Riplet and TRIM25 remains unclear, and the molecular mechanism of how Riplet-mediated RIG-I ubiquitination activates RIG-I signaling remains unresolved.

Hepatitis C virus (HCV) is a major cause of hepatocellular carcinoma (HCC) worldwide. HCV RNA is primarily recognized by RIG-I *in vitro* and *in vivo* [24]. The HCV protease NS3-4A can suppress type I IFN production [25]. NS3-4A cleaves IPS-1 to suppress RIG-I-mediated innate immune responses [7,26]. Human monocyte-derived dendritic cells recognize HCV RNA through Toll-like receptor 3, and NS3-4A has the ability to cleave TICAM-1, which is a solo adaptor molecule of Toll-like receptor 3 [27,28]. In this study, we found that Riplet was another target of NS3-4A. Here, we demonstrated the molecular mechanisms of how Riplet-mediated RIG-I polyubiquitination triggered the type I IFN production signal and showed that this mechanism was targeted by HCV.

Results

Riplet and TRIM25 ubiquitin ligases play different roles in RIG-I activation

In mouse embryonic fibroblasts (MEFs), TRIM25 is essential for type I IFN production in response to SeV infection [15]. As with TRIM25 knockout, Riplet knockout abolished IFN-α2 and IFN-β mRNA expressions in response to SeV infection in MEF (Figure 1A and 1B), which suggested that both ubiquitin ligases were essential for type I IFN expression in MEFs in response to SeV infection. Thus, we examined whether these two ubiquitin ligases played different roles in RIG-I activation.

We performed reporter gene assays with p125luc (IFN-β reporter) using either RIG-I CARDs fragment or full-length RIG-I expression vectors. It is known that ectopic expression of RIG-I CARDs fragment activates the signaling even in the absence of stimulation with RIG-I ligand [2,3] and that the auto-activation is observed when full-length RIG-I is ectopically expressed in HEK293 cell [21,29]. As previously reported, TRIM25 ectopic expression efficiently increased RIG-I CARDs fragment-mediated signaling (Figure 1C). However, TRIM25 expression only mildly increased full-length RIG-I signaling (Figure 1D). In contrast, Riplet ectopic expression efficiently increased the full-length RIG-I-mediated signaling, although Riplet failed to increase the RIG-I CARDs-mediated signaling (Figure 1C and 1D). Interestingly, when Riplet was co-expressed with TRIM25, ectopically expressed TRIM25 could increase the full-length RIG-I-mediated signaling (Figure 1F). We observed the same effects of TRIM25 and Riplet expressions on the reporter activation in the presence of stimulation with HCV 3′ UTR dsRNA (a RIG-I ligand) or VSV infection, which are recognized by RIG-I (Figure 1E and 1F). These different effects of Riplet and TRIM25 on the signaling suggested that Riplet and TRIM25 ubiquitin ligases played different roles in RIG-I activation.

We then investigated whether the two ubiquitin ligases associate with RIG-I after stimulation. First, we performed immunoprecipitation assay and found that endogenous Riplet and TRIM25 bound to endogenous RIG-I after stimulation with HCV dsRNA (Figure 1G). Second, we investigated subcellular localizations of the proteins by confocal immunofluorescence microscopy. In resting cells, RIG-I was barely detectable, whereas RIG-I exhibited punctate staining in cytoplasm after VSV infection (Figure 2A), and ectopically expressed Riplet was co-localized with RIG-I and TRIM25 in perinuclear region in VSV infected cells (Figure 2A–2C and 2E). This is consistent with a previous observation that RIG-I and TRIM25 co-localized extensively at cytoplasmic perinuclear bodies [15]. Pearson's correlation coefficient values also suggested the correlation of the colocalizations of those proteins (Figure 2D and 2F). Recently, it was reported that RIG-I recognized short polyI:C in stress granules [30]. G3BP is a marker of the stress granule [30]. In resting cells, G3BP dispersed in cytoplasm [30], and thus barely detectable (Figure 2G and 2H), whereas G3BP speckles were detected in cells stimulated with short polyI:C in the cytoplasm (Figure 2G and 2H). Riplet and TRIM25 localizations within G3BP speckles were detected in the stimulated cells (Figure 2G and 2H). Taken together, these data indicated that both Riplet and TRIM25 associated with RIG-I after stimulation.

Next, we assessed the RIG-I regions that bind to the two ubiquitin ligases using RIG-I fragments. As previously reported, TRIM25 bound to RIG-I CARDs fragment (Figure 2I). However, Riplet bound to RIG-I RD (735–925 aa), but not to CARDs fragment (Figure 2J). Deleting the Riplet binding region (RIG-I-ΔCTD) abrogated Riplet effect on RIG-I signaling (Figure 2K). This was contrast to TRIM25, which affects RIG-I CARDs. Taken together, our genetic and biochemical data indicated that the two ubiquitin ligases associated with RIG-I after stimulation but showed different effects on RIG-I activation. Thus, we next focused on Riplet specific role in RIG-I activation.

Riplet-mediated RIG-I polyubiquitination is dispensable for RIG-I RNA binding activity

RIG-I CARDs harbor K63-linked polyubiquitination [15]. As RIG-I CARDs, RIG-I RD harbored K63-linked polyubiquitination (Supplemental Figure S1). Riplet expression increased the polyubiquitination of RIG-I RD but not that of CARDs (Figure 3A). RIG-I RD has two functions. One is RNA binding activity and the other is autorepression of its CARDs signaling. Firstly, we tested whether Riplet affects RIG-I RNA binding activity. In a pull-down assay using biotin-conjugated dsRNA and streptavidin beads, we found that both polyubiquitinated and non-ubiquitinated RIG-I were recovered (Figure 3B), which suggested that Riplet-mediated polyubiquitination was dispensable for RIG-I

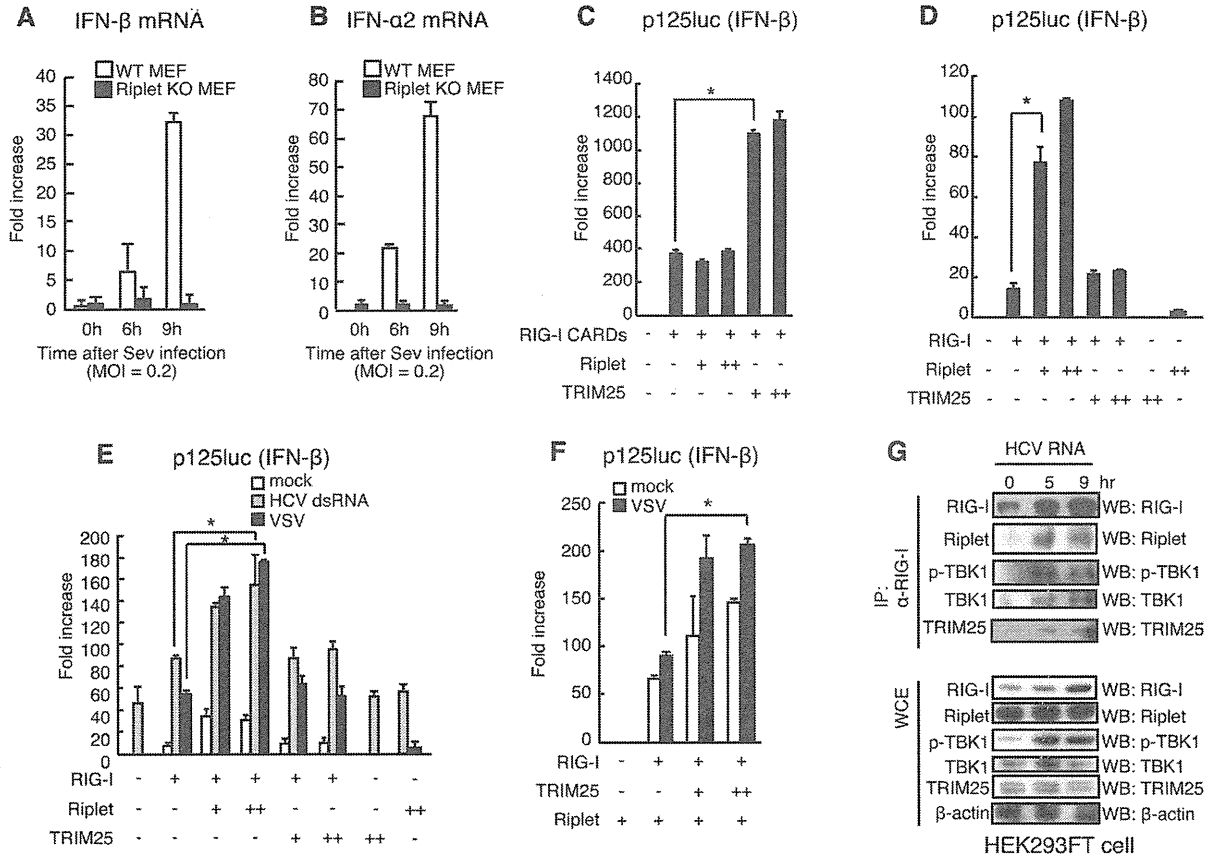

Figure 1. Riplet promotes TRIM25-mediated full-length RIG-I activation. (A, B) Wild-type and Riplet KO MEFs were infected with SeV at MOI = 0.2. The mRNA expressions of IFN-β (A) and -α2 (B) at the indicated times after viral infection were determined by RT-qPCR. Results are presented as mean ± SD (n = 3). (C, D) The activation of IFN-β promoter was examined by reporter gene assay using a p125luc IFN-β reporter. RIG-I CARDs (C) or full-length RIG-I (D) expression vectors were transfected into HEK293 cells together with a Riplet and/or TRIM25 expression vector as indicated. 24 hours after the transfection, the reporter activities were determined. (E, F) The activation of IFN-β promoter was examined by reporter gene assay using a p125luc IFN-β reporter. Full-length RIG-I expression vectors were transfected into HEK293 cells together with a Riplet and/or TRIM25 expression vector as indicated. 24 hours after the transfection, the cells were stimulated with 50 ng of HCV 3′ UTR dsRNA by transfection or infected with VSV at MOI = 1 for 24 hours, and then reporter activation was determined. Data are presented as mean ± SD (n = 3). *$p<0.05$. (G) HEK293FT cells were stimulated with 0.8 μg of HCV double-stranded RNA (HCV RNA) using lipofectamine 2000 in 6-well plate. Cell lysates were prepared at the indicated times, followed by immunoprecipitation with an anti-RIG-I mAb (Alme-1).
doi:10.1371/journal.ppat.1003533.g001

RNA binding activity. As RIG-I is known to form homo-oligomers [3], it is possible that non-ubiquitinated RIG-I was recovered through ubiquitinated RIG-I by the pull-down assay. To exclude this possibility, we used RIG-I mutants, RIG-I 5KR and RIG-I K788R, which were barely ubiquitinated by Riplet (described below). We compared the binding abilities of the RIG-I mutants to that of wild-type RIG-I by pull-down assay using cell lysate isolated from cells without stimulation with RIG-I ligand to avoid any ubiquitination. The results showed that the RIG-I 5KR and RIG-I K788R mutant proteins were recovered by pull down assay as wild-type RIG-I (Figure 3C). This data also indicated that the polyubiquitination is dispensable for RIG-I RNA binding activity.

Riplet releases RIG-I RD autorepression of CARDs signaling

Secondly, we investigated whether Riplet expression affects RIG-I RD autorepression of CARDs signaling. To test this possibility, we constructed RIG-I mutant proteins (Figure 4A). We previously showed that Lys to Ala amino acid substitutions at Lys-849, 851, 888, 907, and 909 of RIG-I (RIG-I 5KA) severely reduced RIG-I polyubiquitination and activation [21]. However, it is possible that the substitutions of Lys with Ala affect other function of RIG-I because the substitution abolishes positive charge of Lys residues. Thus, we constructed the RIG-I 5KR mutant protein, in which the five Lys residues were substituted with Arg, and examined the signal activation ability. The results showed that the 5KR mutation reduced RIG-I signaling, however residual activation of RIG-I 5KR was still detected (Figure 4B–4D). Thus, we assessed other Lys residues within RIG-I RD. Because Riplet is essential for RIG-I activation, it is expected that the Lys residues targeted by Riplet are conserved during evolution. Thus, we tested Lys residues within RIG-I RD conserved among vertebrate, and found that an RIG-I K788R mutation reduced RIG-I signaling at a level comparable to that by a K172R mutation, which abrogates TRIM25-mediated RIG-I activation [15,19] (Figure 4B–4D). Interestingly, the 5KR and K788R

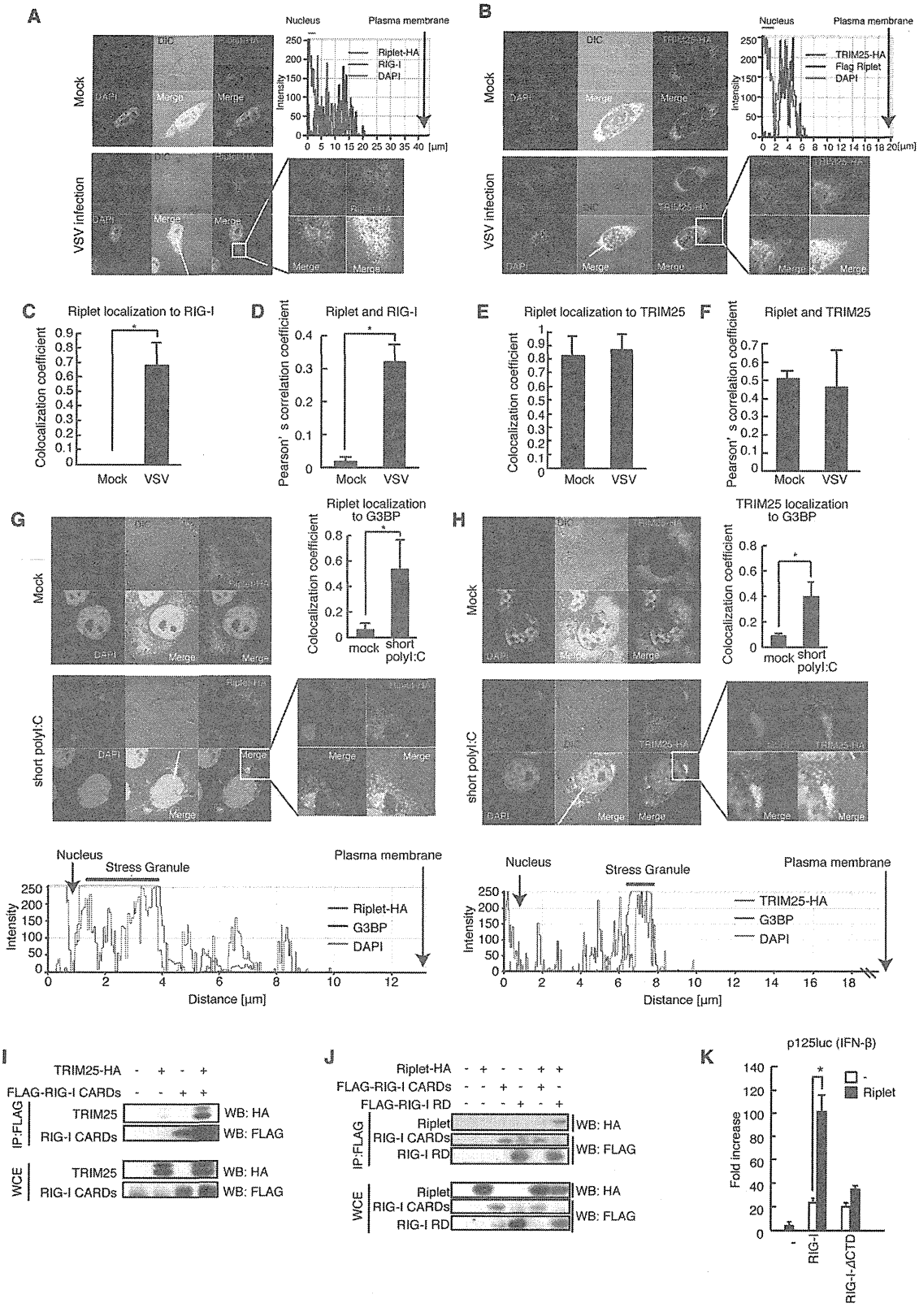
A
Mock
VSV infection
DIC
DAPI
Merge
Riplet-HA
Nucleus
Plasma membrane
Intensity
Riplet-HA
RIG-I
DAPI
[μm]
B
TRIM25-HA
Flag Riplet
C
Riplet localization to RIG-I
Colocalization coefficient
Mock
VSV
D
Riplet and RIG-I
Pearson' s correlation coefficient
E
Riplet localization to TRIM25
F
Riplet and TRIM25
G
Riplet localization to G3BP
mock
short polyI:C
H
TRIM25 localization to G3BP
Stress Granule
G3BP
I
TRIM25-HA
FLAG-RIG-I CARDs
IP:FLAG
WCE
TRIM25
RIG-I CARDs
WB: HA
WB: FLAG
J
Riplet-HA
FLAG-RIG-I RD
Riplet
RIG-I RD
K
p125luc (IFN-β)
Fold increase
RIG-I
RIG-I-ΔCTD

Figure 2. Riplet and TRIM25 ubiquitin ligases associate with RIG-I. (A, B) HeLa cells were transfected with Riplet-HA expression vector (A) or FLAG-Riplet and TRIM25-HA (B). 24 hours after transfection, the cells were infected with VSV at MOI = 1 for six hours. The cells were fixed and stained with anti-RIG-I (Alme-1), HA, and/or FLAG antibodies as indicated. Histograms display the measured fluorescence intensity along the white line in the merged panels. (C–F) Colocalization coefficients of Riplet localization to RIG-I (C) or TRIM25 (E) in mock or VSV infected HeLa cells. Pearson's correlation coefficient of Riplet and RIG-I (D) and TRIM25 (F) (mean ± SD, n>10). (G, H) HeLa cells were transfected with Riplet-HA (G) or TRIM25-HA (H) expression vector. The cells were stimulated with 100 ng of short polyI:C for six hours. The cells were fixed and stained with anti-G3BP and HA antibodies. Colocalization coefficient indicates values (mean ± SD, n>10) of Riplet (G) or TRIM25 (H) localization to G3BP staining region. Histograms display the measured fluorescence intensity along the white line in the merged panels. (I, J) TRIM25 (I) or Riplet (J) expression vector was transfected into HEK293FT cells together with FLAG-tagged-RIG-I CARDs or -RIG-I RD expression vectors. Cell lysate was prepared at 24 hours after transfection, followed by immunoprecipitation with an anti-FLAG antibody. (K) Riplet, RIG-I, and/or RIG-I-ΔRD, which lacks RD, expression vector was transfected into HEK293 cell with p125luc reporter. Reporter activation was determined at 24 hours after transfection. Data are presented as mean ± SD (n = 3).
doi:10.1371/journal.ppat.1003533.g002

mutations reduced the RIG-I polyubiquitination (Figure 4E). RIG-I polyubiquitination in cells stimulated with HCV dsRNA was also reduced by the K788R mutation (Figure 4F). Lys-788 is located within the 55-amino acid region (747–801 aa) of RIG-I essential for RD autorepression of CARDs signaling [31] (Figure 4A). It is possible that the reduction of RIG-I ubiquitination by the mutations was caused by the defect of RIG-I other functions, such as RNA binding activity. However, Figure 3C showed that the RIG-I 5KR and K788R mutant proteins efficiently bound to dsRNA as wild-type RIG-I. This data weakened the above possibility.

Using the RIG-I mutants, we investigated whether Riplet releases RIG-I RD autorepression. Because Riplet ectopic expression activated full-length RIG-I signaling even in the absence of stimulation (Figure 1D), we could assess whether Riplet can remove RIG-I RD autorepression by Riplet ectopic expression study. Due to autorepression, full-length RIG-I expression weakly activates the signaling compared with RIG-I CARDs expression [31]. Riplet ectopic expression increased full-length RIG-I signaling to a level comparable to that of RIG-I CARDs signaling (Figure 5A), suggesting that Riplet released the autorepression. Moreover, the K788R substitution canceled this Riplet ectopic expression effect on RIG-I signaling (Figure 5A). This suggested that the K788R mutation abrogated the release of RIG-I RD autorepression but not RNA binding activity.

Expression of the RIG-I RD fragment is known to represses full-length RIG-I-mediated signaling [3]. Interestingly, Riplet ectopic expression removed the RD fragment repression effect on RIG-I signaling (Figure 5B). This Riplet expression effect was canceled by the K788R amino acid substitution within full-length RIG-I (Figure 5B).

MDA5 C-terminal region does not function as an RD, and thus ectopically expressed MDA5 induced IFN-β promoter activity irrespective of viral infection [3]. If Riplet ectopic expression released RIG-I RD autorepression, it is expected that RIG-I and Riplet co-expression will induce IFN-β promoter activity irrespective of viral infection. As expected, Riplet and RIG-I co-expression induced IFN-β promoter activity irrespective of SeV infection (Figure 5C). Taken together, these genetic data indicated that Riplet released RIG-I RD autorepression.

If Riplet is essential for the release of RIG-I RD autorepression, it is expected that Riplet expression will increase the interaction between RIG-I and TRIM25, because TRIM25 efficiently activated RIG-I CARDs but not full-length RIG-I (Figure 1C and 1D). To test this possibility, we examined the interaction between TRIM25 and RIG-I in the presence or absence of Riplet ectopic expression and found that Riplet expression increased the interaction between TRIM25 and RIG-I (Figure 5D and 5E). Moreover, this interaction was abolished by the K788R mutation (Figure 5F). These data were also consistent with our model that Riplet affects RIG-I RD autorepression rather than RNA binding activity of RIG-I.

If Riplet is essential for the release of RIG-I RD autorepression leading to the interaction between TRIM25 and RIG-I, it was expected that Riplet is essential for endogenous RIG-I K63-linked polyubiquitination that is mediated by both Riplet and TRIM25. To test this possibility, we investigated endogenous RIG-I K63-linked polyubiquitination in mouse spleen cells infected with SeV. Endogenous RIG-I K63-linked polyubiquitination was increased after SeV infection in wild-type splenocyte, however knockout of Riplet abrogated the endogenous K63-linked polyubiquitination of RIG-I after SeV infection (Figure 5G). Recently, it was reported that knockdown of Riplet strongly reduced endogenous RIG-I polyubiquitination in response to SeV infection in a mouse cell line Hepa 1.6 [32]. Based on our genetic and biochemical data in Figure 3–5, we concluded that Riplet affects RIG-I RD autorepression rather than the RNA binding activity.

Riplet is required for the formation of a hetero-protein complex of RIG-I, TBK1, and IKK-ε

Because Riplet-mediated release of RD autorepression increased the interaction between RIG-I and TRIM25, we investigated whether the release of RD autorepression also increased the interaction of RIG-I with other factors. Interestingly, we found that ectopically expressed IKK-ε, TBK1, and NEMO ubiquitin binding region co-immunoprecipitated with RIG-I RD (Figure 6A–6D), and Riplet expression enhanced the physical interactions of RIG-I with TBK1, IKK-ε, and the NEMO ubiquitin binding region (Figure 6D–6G). The physical interactions between these proteins were not through IPS-1, as IPS-1 did not co-immunoprecipitate with RIG-I RD (Figure 6B).

Microscopy analysis showed that the RIG-I was co-localized with TBK1 or NEMO in the cytoplasm. (Figures 6H and S2A). RIG-I and TBK1 was detected in the region where there is no mitochondria (Figure 6I), and the colocalization of RIG-I with TBK1 was also detected in the region where there is no mitochondria (yellow stained region in Figure 6J). This was consistent with our immunoprecipitation results that RIG-I RD could bind TBK1 without IPS-1. TBK1 is phosphorylated in its activation loop [33]. Surprisingly, the phosphorylated TBK1 (p-TBK1) foci were exclusively localized on mitochondria (Figure 6K and 6L). Co-localization of RIG-I with p-TBK1 was observed after dsRNA stimulation (Figure S2B and S2C). We next assessed the role of endogenous Riplet in the interaction between RIG-I and TBK1. Immunoprecipitation assay showed that Riplet KO reduced the interaction between endogenous RIG-I and TBK1 in mouse spleen cells during VSV infection, indicating that Riplet promoted the interaction between RIG-I and TBK1 (Figure 6M). These data indicated that the Riplet function increased the interaction of RIG-I with TBK1 as well as TRIM25.

Hepatitis C virus protease NS3-4A targets the Riplet protein

Several viruses have evolved strategies to escape the innate immunity. For instance, NS1 of influenza A virus inhibits TRIM25 function. This emphasizes the vital role of TRIM25 in

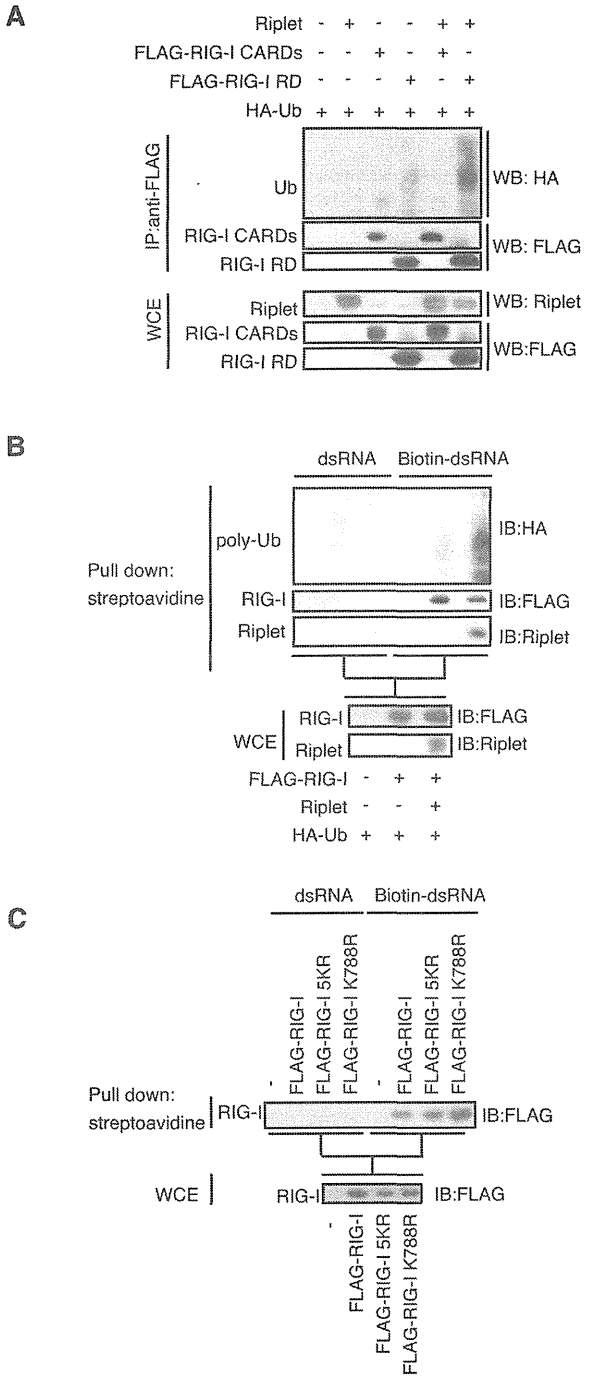

Figure 3. Riplet function is dispensable for RIG-I RNA binding activity. (A) Expression vectors encoding Riplet, FLAG-tagged RIG-I CARDs, and/or FLAG-tagged RIG-I RD were transfected into HEK293FT cells together with an HA-tagged ubiquitin expression vector. Cell lysate was prepared at 24 hours after transfection, followed by immunoprecipitation with an anti-FLAG (RIG-I) antibody. (B) HEK293FT cells were transfected with expression vectors encoding FLAG-tagged RIG-I, Riplet, and HA-tagged ubiquitin. Cell lysate was prepared at 24 hours after transfection, and then incubated with biotin-conjugated (Biotin-dsRNA) or non-conjugated (dsRNA) double-stranded RNA. Biotin-dsRNA was pull-downed with streptavidin beads. Samples were subjected to SDS-PAGE, and proteins were detected by western blotting. (C) HEK293FT cells were transfected with FLAG-tagged wild-type RIG-I, RIG-I 5KR, or RIG-I K788R expression vector. 24 hours after the transfection, the cell lysate was prepared. The pull down assay with biotin-dsRNA was performed as described above.
doi:10.1371/journal.ppat.1003533.g003

modulating antiviral response [34]. To assess the biological significance of Riplet-mediated release of RIG-I RD autorepression in antiviral innate immune response, we investigated whether viral protein suppresses this mechanism.

The endogenous Riplet protein level was not affected by polyI:C, HCV dsRNA stimulations, or by VSV infection (Figure 7A–7C), however the Riplet protein level was severely reduced in a human hepatocyte cell line with HCV 1b full-length replicons (O cells) compared with hepatocyte cell line without these replicons (O curred cells: Oc cells; Figure 7D), suggesting that viral protein reduced the Riplet protein level. Riplet knockout abolished the expression of type I IFN, IP-10, and type III IFN in response to HCV RNA (Figure 7E), indicating that Riplet was essential for type I IFNs expression in response to HCV RNA.

Because HCV protease NS3-4A suppresses type I IFN expression in response to viral infection [7,25], we examined whether NS3-4A could cleave the Riplet protein. N-terminal FLAG-tagged Riplet or C-terminal HA-tagged Riplet was expressed with or without NS3-4A, after which the Riplet protein levels were compared. NS3-4A expression severely reduced the FLAG-tagged and HA-tagged Riplet protein level but not that of FLAG-tagged RIG-I, whereas catalytically inactive NS3-4A* (S139A) failed to reduce the Riplet protein level (Figure 7F, 7G, and S3A). This suggested that this protease's activity reduced the Riplet protein level. Although NS3-4A reduced IPS-1 protein level as previously reported, NS3-4A did not reduce the TRIM25 and IKK-ε protein levels (Figure 7H, 7I, S3B–D).

Within the Riplet RING-finger domain is a sequence that is similar to the NS3-4A target consensus sequence (D/E-x-x-x-x-C/T-S/A; Figure 7J) [35]. NS3-4A cleaves the target just after C/T within this consensus sequence. Acidic amino acids before the C/T site are conserved among the NS3-4A cleavage site within HCV polypeptide. The acidic amino acids from 16 to 18 aa within the Riplet sequence were substituted with Ala, and a Riplet-3A mutant protein was constructed (Figure 7J). The Riplet-3A mutant protein was resistant to NS3-4A (Figure 7I and 7K). Moreover, the Riplet-3A protein co-localized with NS3-4A in cytoplasm (Figure 7L). Interestingly, recombinant NS3-4A that was purified from *E. coli* cleaved the immunoprecipitated FLAG-tagged Riplet protein and recombinant GST-fused Riplet protein purified from *E.coli*, and the cleaved fragments were detected at expected size (Figure 7M and 7N). These data indicated that NS3-4A directly targeted the Riplet protein.

Although Riplet digestion products were not observed in HEK293 cell lysate (Figure S3E and S3F), it is known that the digestion products of TICAM-1 (TRIF) obtained by NS3-4A are not detectable because these products are unstable [28]. Cys-21 of Riplet corresponds to the C/T site in the NS3-4A target consensus sequence. The Cys-21 residue is the first Cys in the RING-finger motif; thus a C21A substitution causes the disruption of RING finger domain structure [36]. The Riplet-C21A mutant protein was unstable and barely detectable (Figure S3G), which suggested that the loss of Cys-21 destabilized the Riplet protein.

HCV protease NS3-4A abolishes an early step of RIG-I activation

To determine if NS3-4A abolishes RIG-I activation by disrupting Riplet, we examined RIG-I ubiquitination and

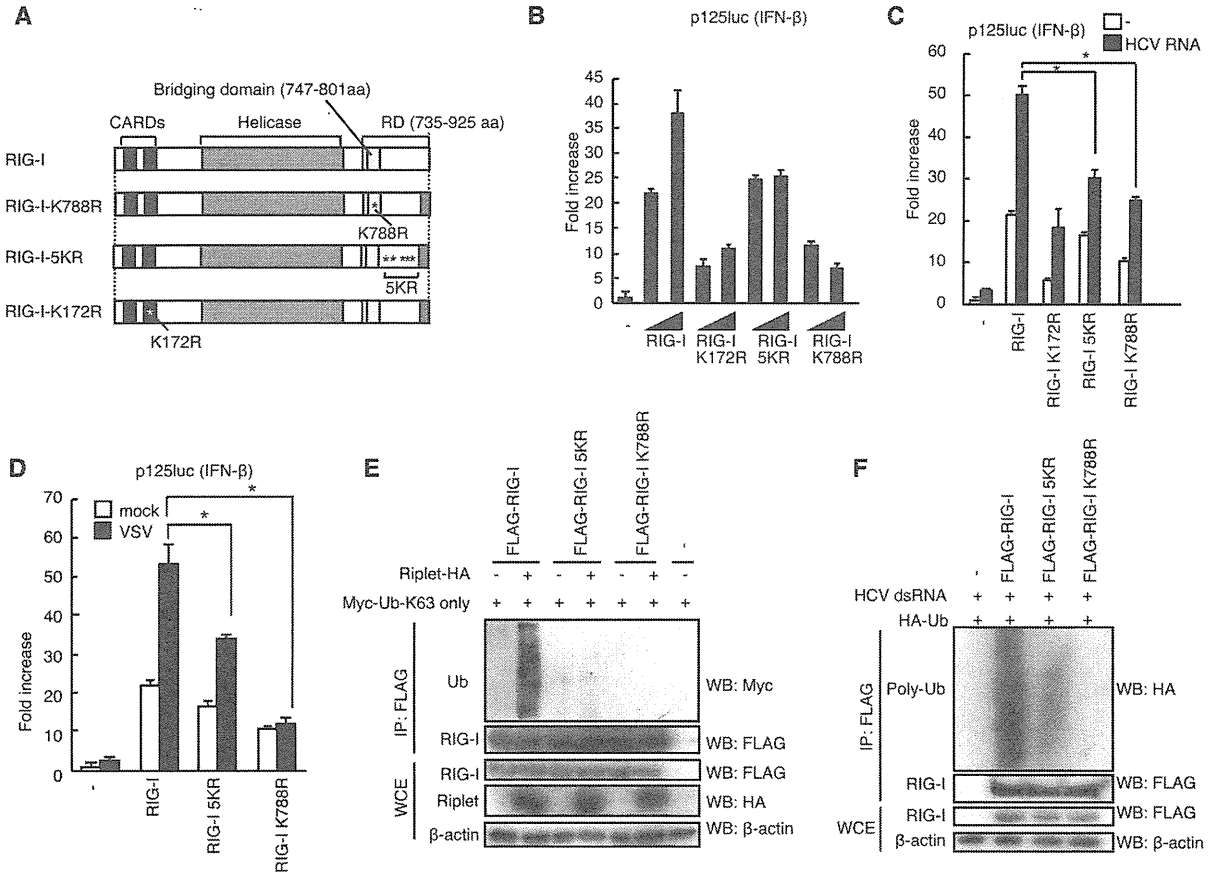

Figure 4. Lys residues within RIG-I RD were essential for Riplet-mediated K63-linked polyubiquitination. (A) Schematic diagram of RIG-I mutant proteins. (B–D) IFN-β promoter activation was determined using a p125luc IFN-β reporter gene. HEK293 cells were transfected with 0.1 μg of expression vectors encoding full-length RIG-I, RIG-I K172R, RIG-I 5KR, and RIG-I K788R in 24-well plate. The transfected cells were stimulated with 0.1 μg of HCV 3′ UTR dsRNA using lipofectamine 2000 reagent for eight hours (C) or infected with VSV at MOI = 1 for 24 hours (D), after which reporter activation was determined. Data are presented as mean ± SD (n = 3). *$p<0.05$. (E) The expression vectors encoding HA-tagged Riplet and FLAG-tagged RIG-I, RIG-I 5KR, and RIG-I K788R were transfected into HEK293FT cells together with Myc-tagged K63-only ubiquitin expression vector, in which all Lys residues except Lys-63 within ubiquitin were replaced with Arg. At 24 hours after transfection, cell lysates were prepared, followed by immunoprecipitation with an anti-FLAG (RIG-I) antibody. (F) The expression vectors encoding FLAG-tagged wild-type and mutant RIG-I proteins were transfected into HEK293FT cells together with HA-tagged ubiquitin expression vector. 24 hours after the transfection, the cells were stimulated with HCV 3′ UTR dsRNA by transfection for eight hours. Then cell lysate was prepared and immunoprecipitation was performed with anti-FLAG antibody.
doi:10.1371/journal.ppat.1003533.g004

interaction between RIG-I and TRIM25. Riplet-mediated ubiquitination of full-length RIG-I or RIG-I RD was abolished by NS3-4A expression (Figure 8A and 8B). K63-linked poly-ubiquitination of RIG-I RD in SeV infected cells were also reduced by NS3-4A expression (Figure 8C). Moreover, NS3-4A expression reduced the interaction between TRIM25 and full-length RIG-I (Figure 8D).

An IPS-1-C508A mutant protein is resistant to NS3-4A cleavage [7]. A reporter gene assay showed that NS3-4A expression severely reduced IFN-β promoter activation induced by RIG-I and Riplet expression even in the presence of the IPS-1 C508A mutant protein in HEK293 cell (Figure 9A), and a catalytically inactive NS3-4A mutant failed to reduce this signal (Figure 9B). These data were consistent with our observation that NS3-4A targeted the Riplet protein. There was endogenous IPS-1 in HEK293 cell, and thus the decrease of IFN-β promoter induction by NS3-4A in HEK293 cell could be due to the cleavage of endogenous IPS-1 by NS3-4A. To exclude this possibility, we next used IPS-1 KO mouse hepatocyte [37]. The IPS-1 C508A mutant protein was expressed in IPS-1 KO hepatocyte. NS3-4A expression reduced the reporter activation induced by RIG-I/Riplet expression or by stimulation with HCV dsRNA even in the presence of IPS-1 C508A (Figure 9C and 9D). These results indicated that NS3-4A targeted both IPS-1 and upstream factors of IPS-1 and were consistent with our observation that NS3-4A reduced the Riplet protein level. We could not test whether NS3-4A failed to impair IFN-β promoter activity in the presence of the Riplet-3A and Riplet C21A mutants because the mutant proteins were not functional and failed to activate RIG-I (Supplemental Figure S3H and S3I). Thus, we could not exclude the possibility that NS3-4A targeted another protein in addition to Riplet and IPS-1.

Hepatitis C virus abrogates endogenous Riplet function

Endogenous RIG-I exhibited punctate staining in the human hepatocyte cell line HuH7 and HepG2 cells after simulation with

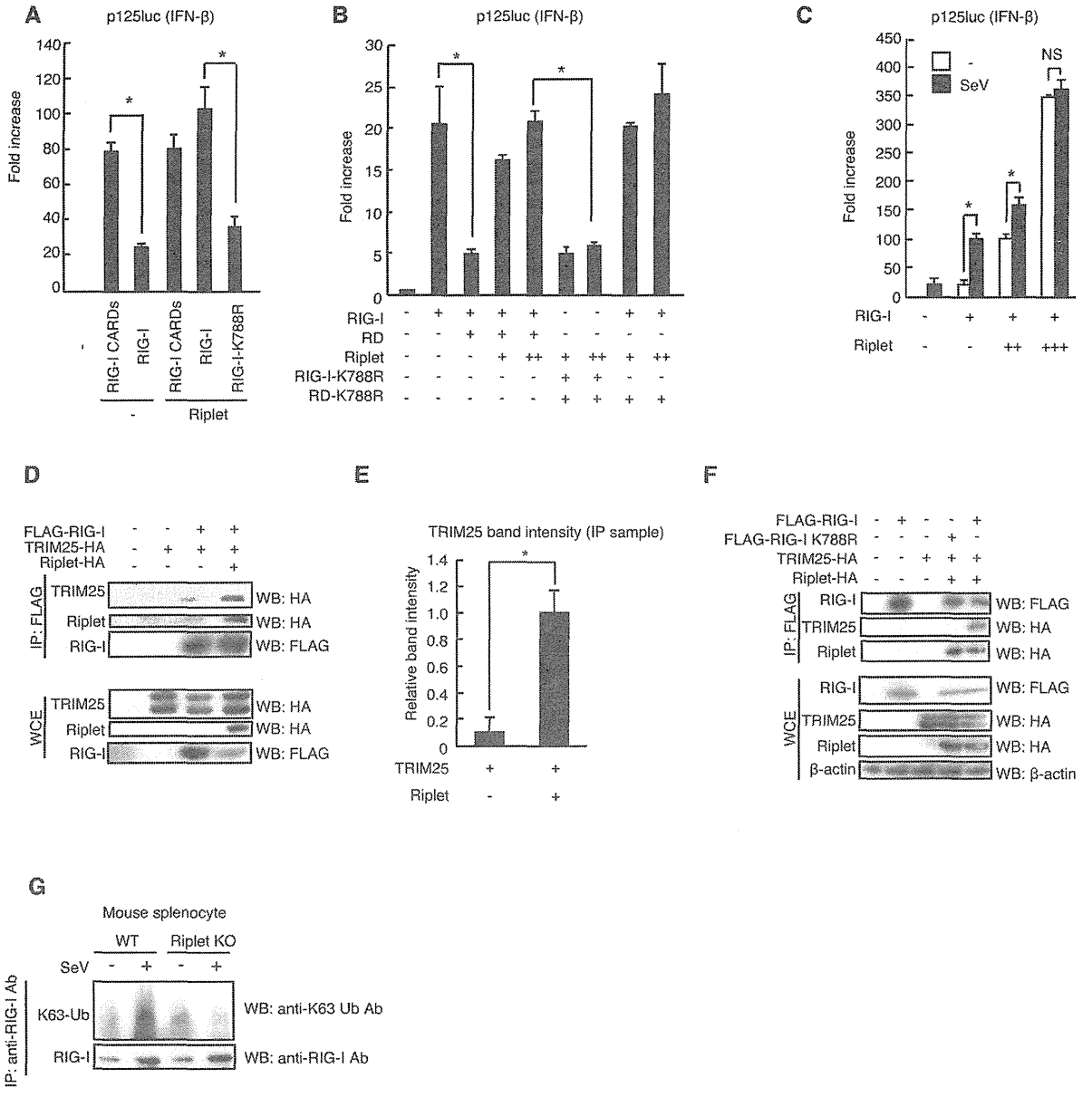

Figure 5. Riplet affects RIG-I RD autorepression of CARDs signaling. (A, B) IFN-β promoter activation was determined using a p125luc IFN-β reporter gene. Expression vectors encoding RIG-I CARDs, full-length RIG-I, RIG-I K788R, RD, RD-K788, and/or Riplet were transfected into HEK293 cells as indicated. Reporter activation was determined after transfection. Data are presented as mean ± SD (n = 3). *$p<0.05$. (C) IFN-β promoter activation was determined using a p125luc IFN-β reporter gene. RIG-I and Riplet expression vectors were transfected into HEK293 cells as indicated. 24 hours after transfection, cells were infected with SeV at MOI = 1 for 24 hours, and the reporter activities were determined. (D–F) HEK293FT cells were transfected with expression vectors encoding FLAG-tagged RIG-I, HA-tagged TRIM25, HA-tagged Riplet, FLAG-tagged RIG-I K788R as indicated. Cell lysate was prepared at 24 hours after transfection, followed by immunoprecipitation with an anti-FLAG antibody (RIG-I). Relative band intensity of immunoprecipitated TRIM25 in panel D was determined (E). (G) Mouse splenocyte was isolated from wild-type and Riplet KO mice spleen. The cells were infected with SeV, and then cell lysate was prepared. Immunoprecipitation was carried out with anti-RIG-I rabbit mAb (D14G6), and subjected to SDS-PAGE. Endogenous K63-linked polyubiquitin chain was detected using K63-linked polyubiquitin chain specific antibody.
doi:10.1371/journal.ppat.1003533.g005

HCV RNA (Figure 9E) but not in HuH7.5 cell line (Figure 9E). In HuH7.5 cells, there is a T55I mutation within endogenous *RIG-I* gene that disrupts the interaction between RIG-I and TRIM25 [38]. We investigated whether Riplet is required for RIG-I to exhibit punctate staining, and found that knockdown of Riplet decreased RIG-I punctate staining induced by HCV RNA (Supplemental Figure S4). We next investigated whether HCV abrogated Riplet-dependent RIG-I punctate pattern in the cytoplasm. As expected, RIG-I failed to exhibit punctate staining in O cells with HCV replicons in NS3 positive cells and HuH7

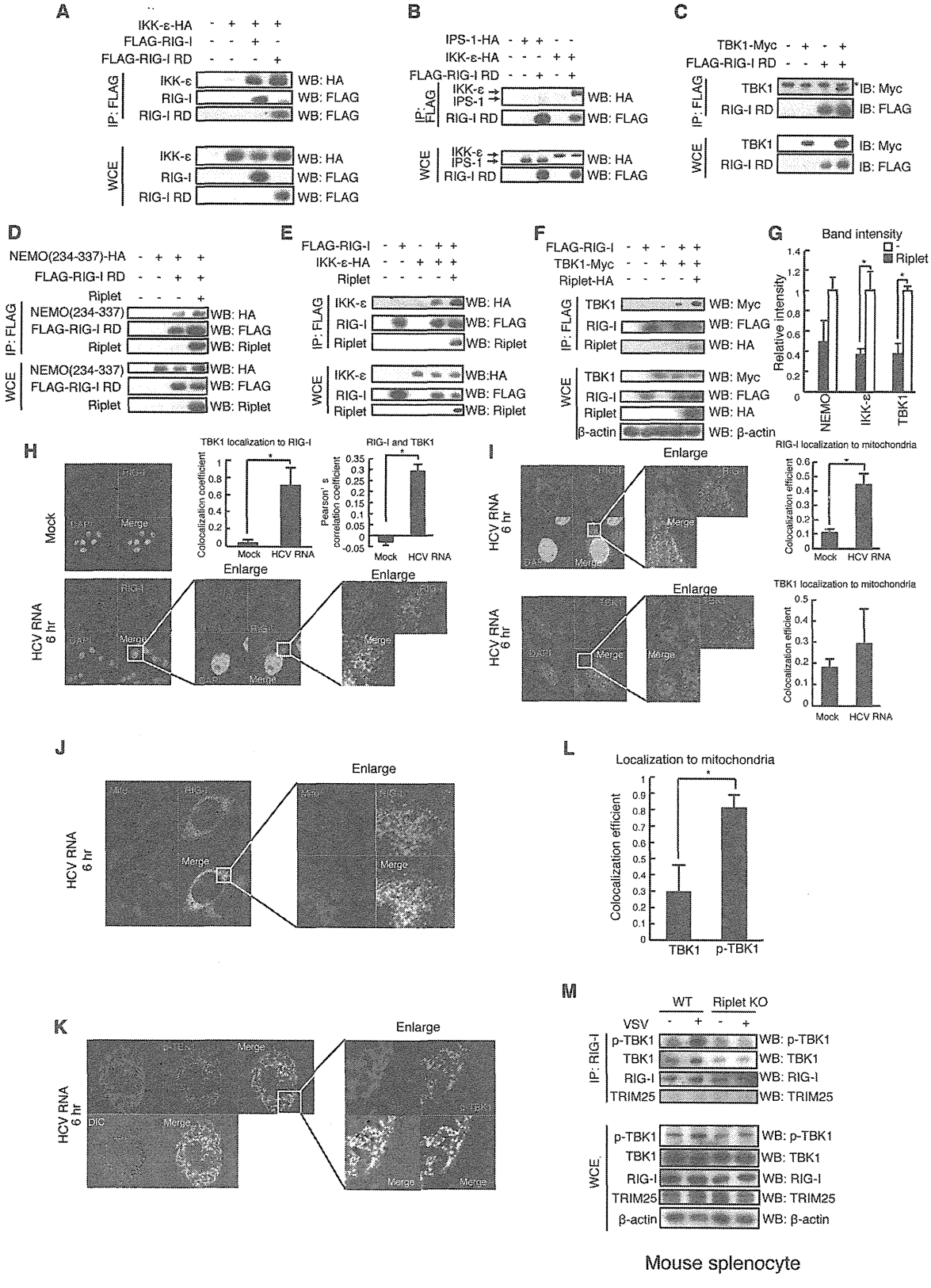
A
IKK-ε-HA - + + +
FLAG-RIG-I - - + -
FLAG-RIG-I RD - - - +
IP: FLAG
IKK-ε
RIG-I
RIG-I RD
WB: HA
WB: FLAG
WB: FLAG
WCE
IKK-ε
RIG-I
RIG-I RD
WB: HA
WB: FLAG
WB: FLAG
B
IPS-1-HA - + + - -
IKK-ε-HA - - - + +
FLAG-RIG-I RD - - + - +
IP: FLAG
IKK-ε
IPS-1
RIG-I RD
WB: HA
WB: FLAG
WCE
IKK-ε
IPS-1
RIG-I RD
WB: HA
WB: FLAG
C
TBK1-Myc - + - +
FLAG-RIG-I RD - - + +
IP: FLAG
TBK1
RIG-I RD
IB: Myc
IB: FLAG
WCE
TBK1
RIG-I RD
IB: Myc
IB: FLAG
D
NEMO(234-337)-HA - + + +
FLAG-RIG-I RD - - + +
Riplet - - - +
IP: FLAG
NEMO(234-337)
FLAG-RIG-I RD
Riplet
WB: HA
WB: FLAG
WB: Riplet
WCE
NEMO(234-337)
FLAG-RIG-I RD
Riplet
WB: HA
WB: FLAG
WB: Riplet
E
FLAG-RIG-I - + - + +
IKK-ε-HA - - + + +
Riplet - - - - +
IP: FLAG
IKK-ε
RIG-I
Riplet
WB: HA
WB: FLAG
WB: Riplet
WCE
IKK-ε
RIG-I
Riplet
WB:HA
WB: FLAG
WB: Riplet
F
FLAG-RIG-I - + - + +
TBK1-Myc - - + + +
Riplet-HA - - - - +
IP: FLAG
TBK1
RIG-I
Riplet
WB: Myc
WB: FLAG
WB: HA
WCE
TBK1
RIG-I
Riplet
β-actin
WB: Myc
WB: FLAG
WB: HA
WB: β-actin
G
Band intensity
Riplet
Relative intensity
NEMO
IKK-ε
TBK1
H
TBK1 localization to RIG-I
RIG-I and TBK1
Colocalization coefficient
Pearson's correlation coefficient
Mock
HCV RNA
Mock
HCV RNA
Enlarge
Enlarge
Mock
HCV RNA 6 hr
RIG-I
DAPI
Merge
I
Enlarge
HCV RNA 6 hr
RIG-I localization to mitochondria
Colocalization efficient
Mock
HCV RNA
Enlarge
TBK1 localization to mitochondria
Colocalization efficient
Mock
HCV RNA
J
Enlarge
HCV RNA 6 hr
Mito
RIG-I
Merge
L
Localization to mitochondria
Colocalization efficient
TBK1
p-TBK1
K
Enlarge
HCV RNA 6 hr
p-TBK1
Merge
DIC
M
WT
Riplet KO
VSV - + - +
IP: RIG-I
p-TBK1
TBK1
RIG-I
TRIM25
WB: p-TBK1
WB: TBK1
WB: RIG-I
WB: TRIM25
WCE
p-TBK1
TBK1
RIG-I
TRIM25
β-actin
WB: p-TBK1
WB: TBK1
WB: RIG-I
WB: TRIM25
WB: β-actin
Mouse splenocyte

Figure 6. The association of TBK1 and IKK-ε protein kinases with RIG-I RD is enhanced by Riplet. (A–F) The interaction of RIG-I with TBK1, IKK-ε, and NEMO was examined by immunoprecipitation assay. FLAG-tagged RIG-I or RIG-I RD expression vector was transfected into HEK293FT cells together with HA-tagged IKK-ε (A, B, and E), Myc-tagged TBK1 (C, F), HA-tagged NEMO ubiquitin binding region (D), and/or Riplet (D–F) expression vectors as indicated. 24 hours after the transfection, cell lysate was prepared, and immunoprecipitation was performed with anti-FLAG antibody. Asterisk indicates non-specific bands. (G) Relative band intensity of immunoprecipitated NEMO, IKK-ε, and TBK1 in D–F was determined. (H–L) Intracellular localization of endogenous RIG-I (H–J), TBK1 (H–J), phosphorylated-TBK1 (p-TBK1) (K), and mitochondria (I–K) were observed using anti-RIG-I (Alme-1), TBK1, p-TBK1 mAbs, and mitotracker. HeLa cells were stimulated with HCV dsRNA for six hours using lipofectamine 2000. Colocalization coefficient of TBK1 localization to RIG-I (H), RIG-I and TBK1 localization to mitochondria (I), and TBK1 and p-TBK1 localization to mitochondria (L) were determined (mean ± sd, n>10). Person's correlation coefficient of RIG-I and TBK1 was determined (H). (M) Splenocytes from wild type and Riplet KO mouse were infected with VSV at MOI = 10 for eight hours. Immunoprecipitation was performed using an anti-RIG-I rabbit monoclonal antibody (D14G6), and the immunoprecipitates were analyzed by SDS-PAGE. Endogenous RIG-I, TBK1, TRIM25, and β-actin were detected using anti-RIG-I, p-TBK1, TRIM25, and β-actin antibodies.
doi:10.1371/journal.ppat.1003533.g006

cells infected with HCV JFH1 (Figure 9F–9H). We confirmed that HCV disrupted IPS-1 in our experimental condition (Figure 9G and 9H).

To further assess whether HCV abrogates endogenous Riplet function, we observed endogenous K63-linked polyubiquitination of RIG-I in cells with HCV replicons. Although SeV infection induced endogenous K63-linked polyubiquitination of RIG-I in HuH7 cells, HCV replicons failed to increase the polyubiquitination (Figure 9I). Next, we investigated the association of endogenous RIG-I with TRIM25 and TBK1, which is promoted by Riplet as shown in Figure 5 and 6. SeV infection induced the association of endogenous RIG-I with TRIM25 and TBK1, whereas HCV replicons failed to induce the association (Figure 9J). Taken together, these data indicated that HCV abrogated endogenous Riplet function.

Although NS3-4A cleaves IPS-1, a mutation within endogenous *RIG-I* gene increased the permissiveness to HCV infection in HuH7-derived cells [3], indicating that RIG-I is required for antiviral response to HCV infection before NS3-4A cleaves IPS-1. We used siRNA to knockdown endogenous Riplet in HuH7 cells, and then the cells were infected with HCV JFH1. Interestingly, Riplet knockdown increased the permissiveness to HCV JFH1 infection (Figure 9K), indicating that endogenous Riplet is required for antiviral response to HCV infection.

Discussion

RIG-I activation is regulated by two ubiquitin ligases Riplet and TRIM25 [15,21]. The two ubiquitin ligases are essential for RIG-I activation [15,23], however the functional difference had been unclear. It is known that TRIM25 is essential for RIG-I oligomerization and association with IPS-1 adaptor molecule [15,19]. Here, we demonstrated that Riplet was essential for the release of RIG-I RD autorepression of its CARDs, which resulted in the association with TRIM25. This functional difference explained the reason why RIG-I requires the two ubiquitin ligases for triggering the signal.

It has been reported that TRIM25 activates RIG-I signaling [15,19]. We confirmed that ectopic expression of TRIM25 increases RIG-I CARDs-mediated signaling. However, most previous studies used a RIG-I CARDs fragment but not full-length RIG-I [15,19,38]. Unexpectedly, we found that the increase of full-length RIG-I-mediated signaling by TRIM25 expression was much less than that of the CARDs-mediated signaling. It is intriguing that Riplet helped TRIM25 to activate full-length RIG-I. Riplet expression promoted the interaction between TRIM25 and full-length RIG-I, and this interaction was abrogated by an RIG-I K788R mutation, which reduced Riplet-mediated RIG-I ubiquitination. Thus, we propose that Riplet-mediated polyubiquitination of RIG-I RD is a prerequisite for TRIM25 to activate RIG-I (Figure 10).

Ectopic expression of Riplet activated RIG-I without stimulation with RIG-I ligand. This is not surprising because ectopically expressed Riplet bound to RIG-I without stimulation with RIG-I ligand, whereas endogenous Riplet bound to endogenous RIG-I after stimulation with RIG-I ligand. RIG-I undergoes its conformational change after binding to a ligand [3,39]. The conformational change would allow the access of endogenous Riplet to RIG-I, which resulted in Riplet-mediated K63-linked polyubiquitination leading to the release of RD autorepression. This model is consistent with the observation that TRIM25 ectopic expression did not activate full-length RIG-I without Riplet expression, because TRIM25 hardly bound to full-length RIG-I without Riplet.

Previously, we reported that the five Lys residues within RIG-I RD were important for Riplet-mediated RIG-I ubiquitination. We constructed the RIG-I 5KR mutant and indicated that the 5KR mutation reduced RIG-I ubiquitination and activation without loss of RNA binding activity. This is consistent with our previous conclusion. However, there is residual ubiquitination of RIG-I 5KR mutation, and we found that K788R mutation showed more sever phenotype. These data indicated that Riplet targeted the several Lys residues within RIG-I RD. This is not surprising, because TRIM25 targets not only Lys-172 but also other Lys residues within mouse RIG-I CARDs [32].

TBK1 and IKK-ε are downstream factors of IPS-1. We found that TBK1 and IKK-ε could bind RIG-I RD. It is possible that RIG-I associates with TBK1 through IPS-1. However, Hiscott J and colleagues demonstrated that IKK-ε could bind IPS-1 and that TBK1 did not bind IPS-1 [40]. Moreover, RIG-I RD did not bind IPS-1, and RIG-I and TBK1 co-localization was detected in the cytoplasmic region where there are no mitochondria. These observations weaken this possibility. Our results indicated that RIG-I RD bound to the NEMO ubiquitin binding region. IRF-3 activation requires the ubiquitin binding domain of NEMO, and an endogenous K63-linked polyubiquitin chain plays a key role in IRF3 activation [41]. Thus, we prefer a model in which TBK1 associates with an RIG-I RD-anchored polyubiquitin chain through NEMO (Figure 10). Although Riplet knockout reduced the binding of RIG-I to TBK1, residual binding was still detectable. Thus, there appears to be Riplet-dependent and independent associations between RIG-I and TBK1. TRAF3 is an E3 ubiquitin ligase, and is involved in the RIG-I-mediated type I IFN production pathway [42]. Because there is residual activation of the type I IFN production pathway even in TRAF3 knockout cells [41], it is possible that the RIG-I polyubiquitin chain may compensate for the TRAF3 defect in recruiting TBK1 to mitochondria. Further studies will be needed to determine the precise molecular mechanisms. Although TBK1 dispersed in the cytoplasm, p-TBK1 was exclusively localized on mitochondria. Considering that TBK1 is phosphorylated in its activation loop [33], these results suggested that RIG-I RD associated with

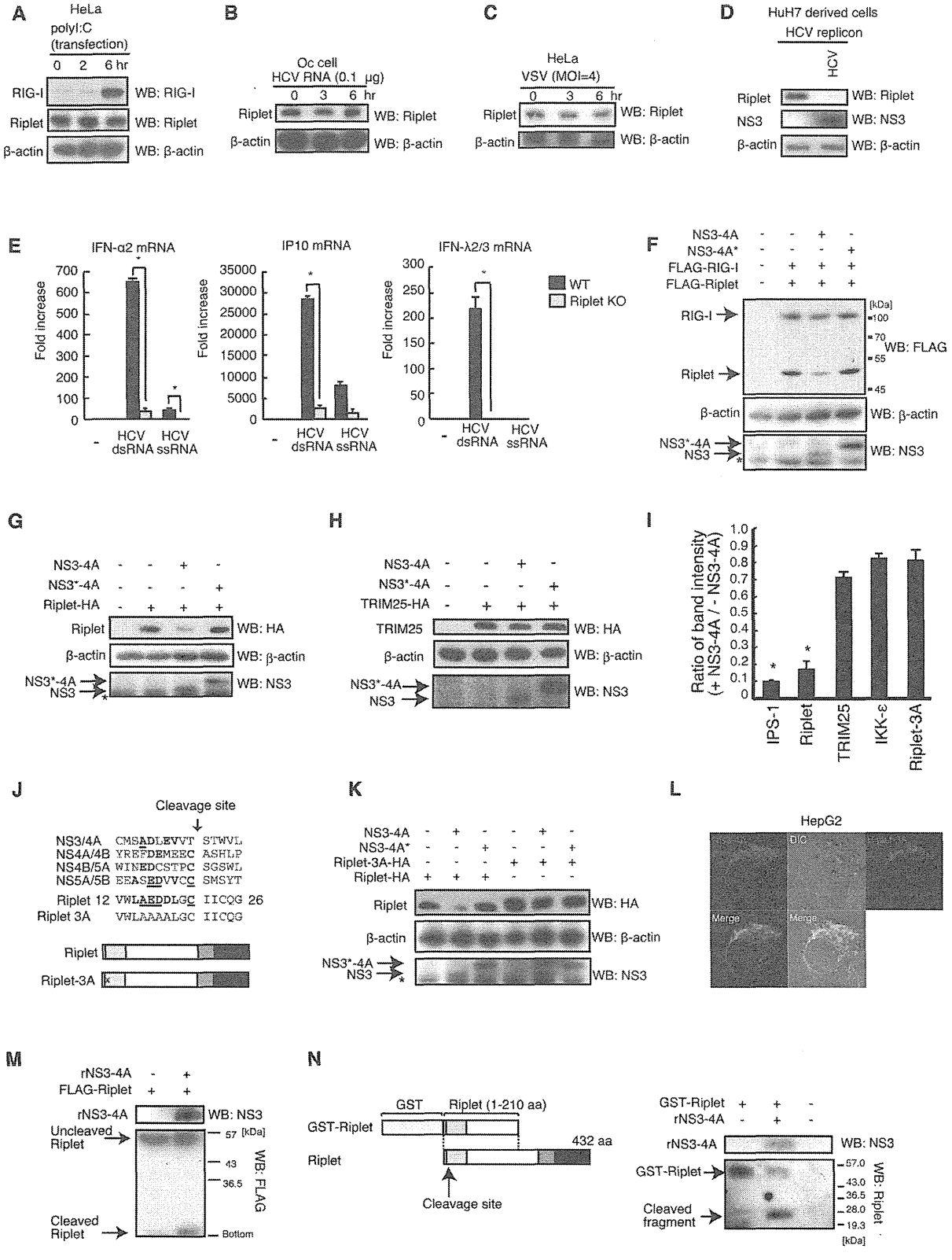
A
HeLa
polyI:C
(transfection)
0 2 6 hr
RIG-I
Riplet
β-actin
WB: RIG-I
WB: Riplet
WB: β-actin
B
Oc cell
HCV RNA (0.1 μg)
0 3 6 hr
Riplet
β-actin
WB: Riplet
WB: β-actin
C
HeLa
VSV (MOI=4)
0 3 6 hr
Riplet
β-actin
WB: Riplet
WB: β-actin
D
HuH7 derived cells
HCV replicon
HCV
Riplet
NS3
β-actin
WB: Riplet
WB: NS3
WB: β-actin
E
IFN-α2 mRNA
IP10 mRNA
IFN-λ2/3 mRNA
Fold increase
WT
Riplet KO
- HCV dsRNA HCV ssRNA
F
NS3-4A
NS3-4A*
FLAG-RIG-I
FLAG-Riplet
RIG-I
Riplet
β-actin
NS3*-4A
NS3
[kDa]
100
70
55
45
WB: FLAG
WB: β-actin
WB: NS3
G
NS3-4A
NS3*-4A
Riplet-HA
Riplet
β-actin
NS3*-4A
NS3
WB: HA
WB: β-actin
WB: NS3
H
NS3-4A
NS3*-4A
TRIM25-HA
TRIM25
β-actin
NS3*-4A
NS3
WB: HA
WB: β-actin
WB: NS3
I
Ratio of band intensity
(+ NS3-4A / - NS3-4A)
IPS-1
Riplet
TRIM25
IKK-ε
Riplet-3A
J
Cleavage site
NS3/4A CMSADLEVVT STWVL
NS4A/4B YREFDEMEEC ASHLP
NS4B/5A WINEDCSTPC SGSWL
NS5A/5B EEASEDVVCC SMSYT
Riplet 12 VWLAEDDLGC IICQG 26
Riplet 3A VWLAAAALGC IICQG
Riplet
Riplet-3A
K
NS3-4A
NS3-4A*
Riplet-3A-HA
Riplet-HA
Riplet
β-actin
NS3*-4A
NS3
WB: HA
WB: β-actin
WB: NS3
L
HepG2
DIC
Merge
Merge
M
rNS3-4A
FLAG-Riplet
rNS3-4A
Uncleaved Riplet
Cleaved Riplet
57 [kDa]
43
36.5
Bottom
WB: NS3
WB: FLAG
N
GST
Riplet (1-210 aa)
GST-Riplet
Riplet
432 aa
Cleavage site
GST-Riplet
rNS3-4A
rNS3-4A
GST-Riplet
Cleaved fragment
57.0
43.0
36.5
28.0
19.3
[kDa]
WB: NS3
WB: Riplet

Figure 7. NS3-4A of HCV targets the Riplet protein. (A–D) Endogenous RIG-I and Riplet protein levels were observed by western blotting. HeLa cells were stimulated with polyI:C transfection (A), HCV dsRNA transfection (B) or infected with VSV (C). HCV replicon positive (HCV) and negative (-) cell lysates were prepared from a HuH7-derived cell line O cell that contains HCV 1b full-length replicons and O curred cell (Oc cell) in which HCV replicons were removed by IFN treatment (D). (E) The response to HCV RNA in wild-type and Riplet KO MEFs was examined by RT-qPCR. Wild type (WT) and Riplet knockout (KO) MEF cells were transfected with 100 ng of HCV ssRNA and dsRNA. Six hours after stimulation, mRNA expressions of IFN-α2, IP10, and IFN-λ2/3 were measured by RT-qPCR. Data are presented as mean ± SD (n = 3). *$p<0.05$. (F–H) FLAG-tagged Riplet and RIG-I (F), HA-tagged Riplet (G), or HA-tagged TRIM25 (H) expression vectors were transfected into HEK293FT cells together with NS3-4A or NS3-4A* expression vectors. NS3-4A* mutant protein harbors an amino acids substitution at its catalytic site Ser-139 with Ala. 24 hours after transfection, cell lysate was prepared and subjected to SDS-PAGE. (I) Band intensity ratio of IPS-1, Riplet, TRIM25, IKK-ε, and Riplet-3A with/without NS3-4A expression (mean ± sd, n = 3). (J) NS3-4A cleavage sites within an HCV polypeptide are compared with a candidate site in the Riplet RING-finger domain. Homologous amino acids are shown in bold, and identical amino acids are underlined. In Riplet-3A mutant protein, three acidic amino acids, Glu-16, Asp-17, Asp-18, were substituted with Ala. (K) An expression vector encoding wild-type Riplet or Ripled-3A mutant protein was transfected into HEK293 cells together with NS3-4A or NS3-4A* expression vectors. Cell lysate was prepared 24 hours after transfection, and subjected to SDS-PAGE. (L) HA-tagged Riplet-3A and NS3-4A expression vectors were transfected into HepG2 cell. 24 hours after transfection, the cells were fixed and stained with anti-HA monoclonal antibody (mouse) and anti-NS3-4A polyclonal antibody (goat). (M) N-terminal FLAG-tagged Riplet was expressed in HEK293FT cells, and immunoprecipitation was carried out with anti-FLAG antibody. Immunoprecipitates were incubated with recombination NS3-4A purified from *E.coli* at 37°C for one hour, and samples were subjected to SDS-PAGE analysis. The proteins were detected by western blotting. (N) Purified GST fused Riplet (1–210 aa) was incubated with or without recombinant NS3-4A (rNS3-4A) at 37°C for 30 min. The proteins were subjected to SDS-PAGE and detected by western blotting.

doi:10.1371/journal.ppat.1003533.g007

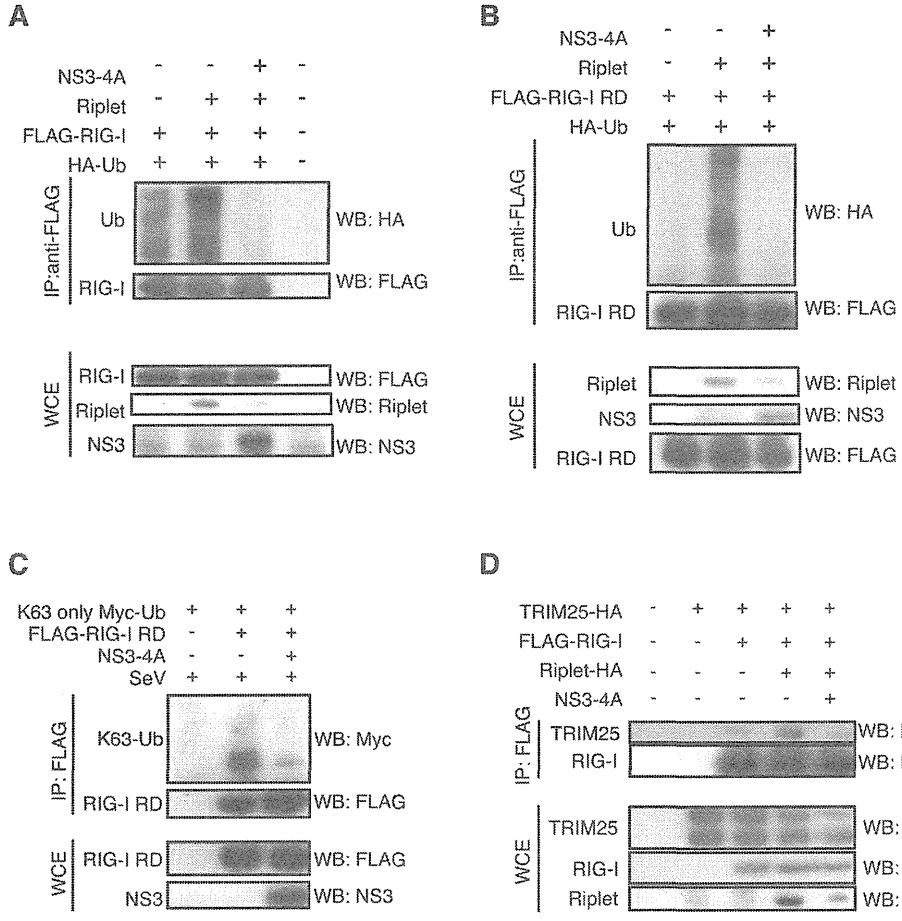

Figure 8. NS3-4A inhibits Riplet-mediated RIG-I polyubiquitination. (A, B) Riplet, NS3-4A, and/or HA-tagged ubiquitin (HA-Ub) expression vectors were transfected into HEK293FT cells along with either full-length RIG-I (A) or RIG-I RD (B). Cell lysate was prepared 24 hours after transfection, and subjected to SDS-PAGE. The proteins were detected by western blotting. (C). HEK293FT cells were transfected with Myc-tagged K63-only ubiquitin, FLAG-tagged RIG-I RD, and/or NS3-4A expression vectors. 24 hours after the transfection, cells were infected with SeV for six hours, and then cell lysate was prepared. Immunoprecipitation was carried out with anti-FLAG antibody, and the samples were subjected to SDS-PAGE. (D) HA-tagged TRIM25, Riplet and/or FLAG-tagged RIG-I expression vectors were transfected into HEK293FT cells with or without NS3-4A expression vector. Cell lysate was prepared 24 hours after the transfection, and immunoprecipitation assay was performed with anti-FLAG antibody. The precipitates were subjected to SDS-PAGE.

doi:10.1371/journal.ppat.1003533.g008

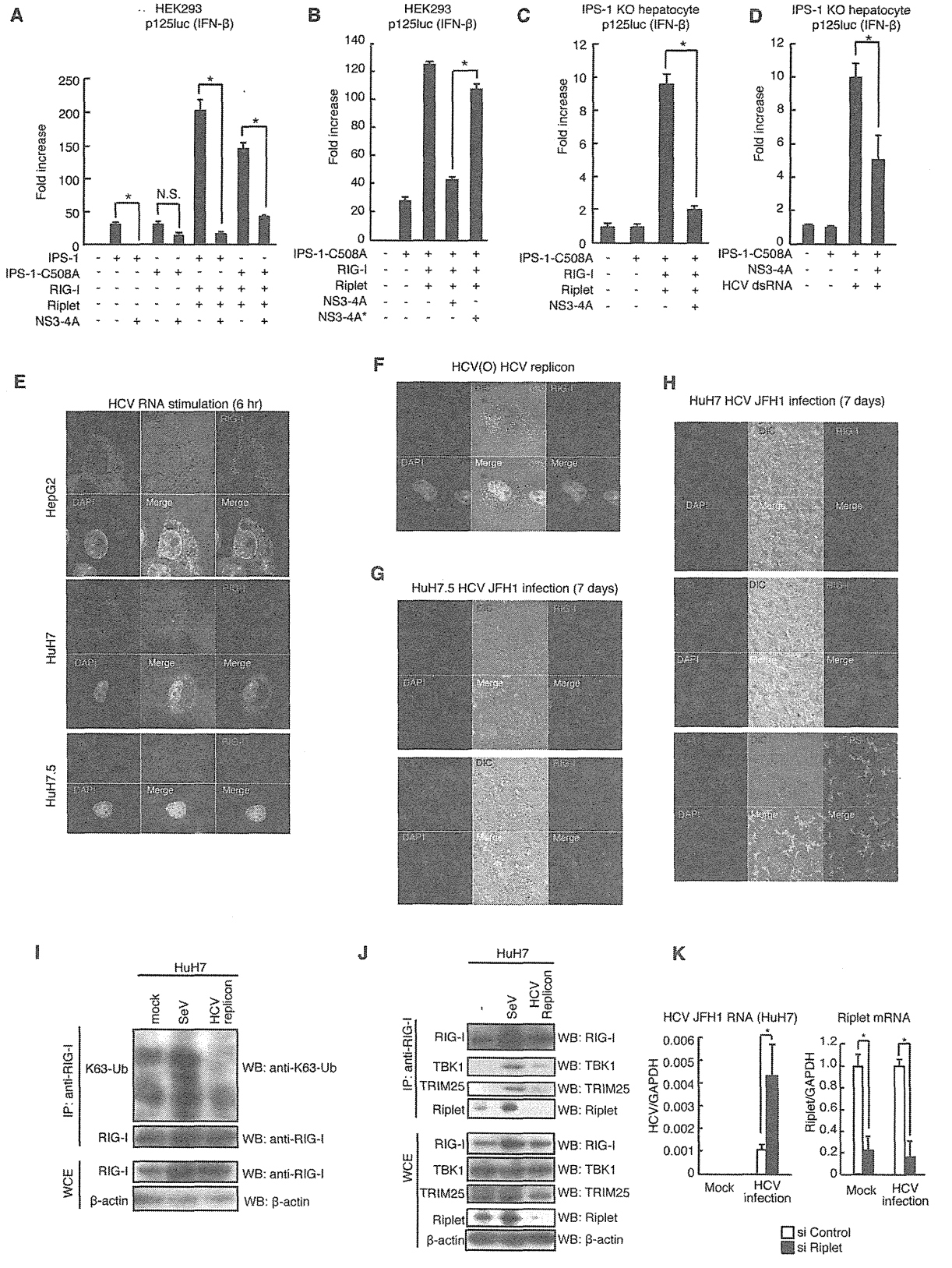
A
HEK293
p125luc (IFN-β)
Fold increase
N.S.
IPS-1
IPS-1-C508A
RIG-I
Riplet
NS3-4A
B
HEK293
p125luc (IFN-β)
Fold increase
IPS-1-C508A
RIG-I
Riplet
NS3-4A
NS3-4A*
C
IPS-1 KO hepatocyte
p125luc (IFN-β)
Fold increase
IPS-1-C508A
RIG-I
Riplet
NS3-4A
D
IPS-1 KO hepatocyte
p125luc (IFN-β)
Fold increase
IPS-1-C508A
NS3-4A
HCV dsRNA
E
HCV RNA stimulation (6 hr)
HepG2
HuH7
HuH7.5
DAPI
Merge
RIG-I
F
HCV(O) HCV replicon
G
HuH7.5 HCV JFH1 infection (7 days)
H
HuH7 HCV JFH1 infection (7 days)
I
HuH7
mock
SeV
HCV replicon
IP: anti-RIG-I
K63-Ub
RIG-I
WCE
β-actin
WB: anti-K63-Ub
WB: anti-RIG-I
WB: β-actin
J
HuH7
SeV
HCV Replicon
IP: anti-RIG-I
TBK1
TRIM25
Riplet
WCE
WB: RIG-I
WB: TBK1
WB: TRIM25
WB: Riplet
WB: β-actin
K
HCV JFH1 RNA (HuH7)
HCV/GAPDH
Riplet mRNA
Riplet/GAPDH
Mock
HCV infection
si Control
si Riplet

Figure 9. HCV abrogated Riplet-mediated RIG-I activation. (A and B) The inhibition of IFN-β promoter activation by NS3-4A was assessed by reporter gene assays. IPS-1-C508A mutant protein harbors an amino acid substitution at Cys-508 with Ala. 100 ng of IPS-1, IPS-1-C508A, RIG-I, Riplet, NS3-4A, and/or NS3-4A* expression vectors were transfected into HEK293 cells in 24-well plates with p125luc reporter plasmid. The total amount of transfected DNA (800 ng/well) was kept constant by adding empty vector (pEF-BOS). 24 hours after the transfection, the reporter activities were measured. Data are presented as mean ± SD (n = 3). *p<0.05. (C and D) IPS-1 KO mouse hepatocyte was transfected with IPS-1 C508A, RIG-I, Riplet, and/or NS3-4A expression vectors together with p125luc and *Renilla* luciferase plasmids. Transfected cells were stimulated with 50 ng of HCV dsRNA for 24 hours by transfection (D). Data are presented as mean SD (n = 3). *p<0.05. (E and F) Intracellular localizations of endogenous TBK1 and RIG-I were determined by confocal microscopy. HepG2, HuH7, and HuH7.5 cells were stimulated with 100 ng of HCV dsRNA for six hours by transfection (E). Stimulated cells (E) and O cells with HCV replicons (F) were stained with anti-RIG-I, TBK1, and/or NS3 antibodies. (G and H) HuH7 (G) and HuH7.5 (H) cells were infected with HCV JFH1 strain. Seven days after the infection, the cells were stained with anti-RIG-I, IPS-1, and NS3 antibodies. (I) HuH7 cells were infected with SeV at MOI = 1 for 24 hours. Cell lysates were prepared from mock or SeV infected HuH7 or HuH7 cells with HCV replicons (O cell). Immunoprecipitation using high salt buffer was performed with anti-RIG-I (Alme-1) antibody. The samples were subjected to SDS-PAGE. Endogenous K63-linked polyubiquitin chain was detected using ubiquitin K63-linkage specific antibody. (J) HuH7 cells were infected with SeV at MOI = 1 for 24 hours. Cell lysates were prepared from mock or SeV infected HuH7 or HuH7 cells with HCV replicons (O cell). Immunoprecipitation was performed with anti-RIG-I (Alme-1) antibody. The samples were subjected to SDS-PAGE. (K) HuH7 cells were transfected with siRNA for mock or Riplet. 48 hours after the transfection, cells were infected with HCV JFH1 for 2 days. RT-qPCR was performed to determine HCV genome RNA, GAPDH, and Riplet expression.
doi:10.1371/journal.ppat.1003533.g009

inactive TBK1 and that TBK1 was activated after loading on to mitochondria (Figure 10).

HCV is a major cause of HCC and has the ability to evade host innate immune response [7,43]. HCV RNA is primarily recognized by the cytoplasmic viral RNA sensor RIG-I. Previous studies showed that the protease NS3-4A cleaves IPS-1 to shut off RIG-I signaling. However, our results indicated that there was another target of NS3-4A in RIG-I signaling. First, RIG-I failed to exhibit punctate staining in cells infected with HCV. Second, NS3-4A reduced RIG-I signaling even in the presence of an IPS-1-C508A mutant, which is resistant to the cleavage by NS3-4A. Third, the endogenous Riplet protein level was severely reduced in cells with HCV replicons. Fourth, NS3-4A targeted Riplet and abrogated Riplet-dependent RIG-I ubiquitination and complex formation with TRIM25 and TBK1. These data support our model that NS3-4A targets not only IPS-1 but also Riplet to escape host innate immune responses (Figure 10). Recently it was reported that NS1 proteins of Influenza A virus inhibited Riplet function [32]. These findings indicated biological importance of Riplet in RIG-I activation during viral infection.

In general, a ubiquitin ligase has several targets. We have performed yeast two-hybrid screening using Riplet as bait and found a candidate clone that encodes a tumor suppressor gene. Our pilot study showed that Riplet mediated K63-linked polyubiquitination of this tumor suppressor and suppressed retinoblastoma (Rb) activity. Thus, Riplet disruption by NS3-4A might be a cause of liver disease induced by HCV infection.

Materials and Methods

Ethics statement

All animal studies were carried out in strict accordance with Guidelines for Animal Experimentation of the Japanese Associations for Laboratory Animal Science. The protocols were approved by the Animal Care and Use Committee of Hokkaido University, Japan (Permit Number: 08-0245 and 09-0215).

Cell

HEK293, Vero, and HepG2 cells were cultured in Dulbecco's modified Eagle's medium low glucose medium (D-MEM) with 10% heat-inactivated fetal calf serum (FCS) (Invitrogen). HeLa cells were cultured in minimum Eagle's medium with 2 mM L-glutamine and 10% heat-inactivated FCS. HEK293FT cells were maintained in D-MEM high glucose medium containing 10% of heat-inactivated FCS (Invitrogen). Human hepatocyte cell line with HCV 1b full-length replicons (O cells) and O curred cells (Oc cells) were kindly gifted from Kato N [44]. O cells were cultured in D-MEM high glucose with 10% of heat-inactivated FCS, G418, NEAA, and L-Gln.

Viruses

VSV Indiana strain and SeV HVJ strain were amplified using Vero cells. To determine the virus titer, we performed plaque assay using Vero cells. HCV JFH1 was amplified using HuH7.5 cells.

Mice

Generation of IPS-1 KO and Riplet KO mice were described previously [23,45]. Splenocyte was isolated from C57BL/6 wild-type and Riplet KO mice. Isolated cells were cultured in RPMI1640 containing 10% of heat-inactivated FCS. The preparations of wild-type and Riplet KO MEFs were described previously [23]. Preparation of IPS-1 KO mouse hepatocyte was described previously [37]. All mice were maintained under specific-pathogen free conditions in the animal facility of the Hokkaido University Graduate School of Science (Japan).

Plasmids

Expression vectors encoding for N-terminal FLAG-tagged RIG-I, N-terminal FLAG-tagged RIG-I CARDs (dRIG-I), FLAG-tagged RIG-I ΔRD (RIG-I-dRD), FLAG-tagged RIG-I RD, C-terminal HA-tagged TRIM25, C-terminal HA-tagged Riplet, and Riplet-ΔRING (Riplet-DN) plasmids were described previously [21,23]. The amino acids substitutions from 16 to 18 with Ala was carried out by PCR-mediated mutagenesis using primers, Ripelt-3A-F and Riplet-3A-R and pEF-BOS/Riplet plasmid as a template. The primer sequence is Riplet-3A-F: TTC CCG TGT GGC TGG CCG CGG CCG CCC TCG GCT GCA TCA TCT GCC, and Riplet-3A-R: GGC AGA TGA TGC AGC CGA GGG CGG CCG CGG CCA GCC ACA CGG GAA. RIG-I K172R and RIG-I K788R expression vectors was constructed by PCR-mediated mutagenesis using primers, RIG-I K172R-F, RIG-I K172R-R, RIG-I K788R-F and RIG-I-K788R-R, and pEF-BOS/FLAG-RIG-I plasmid as a template. The primer sequences are RIG-I K172R-F: GGA AAA CTG GCC CAA AAC TTT GAG ACT TGC TTT GGA GAA AG, RIG-I K172R-R: CTT TCT CCA AAG CAA GTC TCA AAG TTT TGG GCC AGT TTT CC, RIG-I-K788R-F: TGC ATA TAC AGA CTC ATG AAA GAT TCA TCA GAG ATA GTC AAG AA, and RIG-I-K788-R: CTT GAC TAT CTC TGA TGA ATC TTT CAT GAG TCT GTA TAT GCA G. RIG-I 5KR expression vectors were constructed by PCR-mediated mutagenesis using primers, RIG-I 849 851 RR-F, RIG-I 849 851 RR-R, RIG-I 888R-F, RIG-I 888R-R, RIG-I 907 909 RR-F, RIG-I 907 909 RR-R, and